Ocean Modelling 110 (2017) 32–48

Contents lists available at ScienceDirect

Ocean Modelling

journal homepage: www.elsevier.com/locate/ocemod

# Benchmarking an unstructured grid sediment model in an energetic estuary

Jesse E. Lopez*, António M. Baptista

*NSF Science and Technology Center for Coastal Margin Observation & Prediction, Oregon Health & Science University, Portland, OR, USA*

ARTICLE INFO

*Article history:*
Received 20 April 2016
Revised 9 November 2016
Accepted 13 December 2016
Available online 14 December 2016

*Keywords:*
Sediment model
Model validation
Sediment dynamics
Estuaries
Columbia River

ABSTRACT

A sediment model coupled to the hydrodynamic model SELFE is validated against a benchmark combining a set of idealized tests and an application to a field-data rich energetic estuary. After sensitivity studies, model results for the idealized tests largely agree with previously reported results from other models in addition to analytical, semi-analytical, or laboratory results. Results of suspended sediment in an open channel test with fixed bottom are sensitive to turbulence closure and treatment for hydrodynamic bottom boundary. Results for the migration of a trench are very sensitive to critical stress and erosion rate, but largely insensitive to turbulence closure. The model is able to qualitatively represent sediment dynamics associated with estuarine turbidity maxima in an idealized estuary. Applied to the Columbia River estuary, the model qualitatively captures sediment dynamics observed by fixed stations and shipborne profiles. Representation of the vertical structure of suspended sediment degrades when stratification is underpredicted. Across all tests, skill metrics of suspended sediments lag those of hydrodynamics even when qualitatively representing dynamics. The benchmark is fully documented in an openly available repository to encourage unambiguous comparisons against other models.



## 1. Introduction

Sediment dynamics of estuaries control morphodynamic and biogeochemical processes with implications ranging from ecosystem function and health (Ferguson et al., 1996) to navigation (Meade, 1972) among other aspects of system sustainability, management and operation. Driven by tides and buoyancy, estuarine circulation commonly leads to a complex vertical structure of density and currents requiring three-dimensional modeling to represent the inherently depth-varying circulation and sediment processes. As a consequence, sediment modules have been developed for existing three-dimensional circulation models including structured grid models such as Delft3D (Lesser et al., 2004) and ROMS (Warner et al., 2008) and unstructured grid models including FVCOM (Chen et al., 2003), SUNTANS (Fringer et al., 2006), and SELFE (Zhang & Baptista, 2008) and its derivative SCHISM (Zhang et al., 2016). Regardless of the grid structure and specific numerics, sediment modeling systems generally solve the advection-diffusion equation for a user-defined number of suspended sediment classes with distinct approaches for boundary conditions, interactions with bathymetry, and bed load transport.

Validation of sediment models has consisted predominantly of idealized cases with assessments against analytical or laboratory results. Open channel cases without density effects requiring reproduction of a Rouse profile are a common test to evaluate suspended sediment dynamics (Lesser et al., 2004; Pinto et al., 2012; Warner et al., 2008). The trench migration test case of van Rijn (1986) is commonly used to evaluate simulation skill for predictive bedload and morphodynamic behavior (Lesser et al., 2004; Pinto et al., 2012; Warner et al., 2008). Idealized estuarine test cases that include density effects have been used to evaluate sediment behavior in controlled conditions, but lack quantitative solutions (Burchard & Baumert, 1998; Warner et al., 2008). Validation tests inclusive of short wave effects include both laboratory experiments (Lesser et al., 2004) and comparisons against field observations (Warner et al., 2008).

Realistic applications of suspended sediment models are frequently used to study processes associated with estuarine turbidity maxima (ETM). Brenon & Hir (1999) studied the development of the Seine ETM using a single non-cohesive class with a parameterization derived from literature values. Burchard et al. (2004) used a single non-cohesive class characteristic of that system to simulate and study the Elbe ETM using GETM. Lin et al. (2003) characterized the ETM and a secondary turbidity maximum in the York River using a single non-cohesive class with other parameterizations

* Corresponding author.
*E-mail address:* lopezjes@ohsu.edu (J.E. Lopez).

http://dx.doi.org/10.1016/j.ocemod.2016.12.006

derived from sensitivity studies. de Nijs & Pietrzak (2012) evaluated the skill of Delft3D to represent the characteristics of multiple ETMs in the stratified Rotterdam Waterway in realistic conditions using a single non-cohesive sediment size class, with the derivation of sediment parameterization details not disclosed. Ralston et al., (2012) used four non-cohesive classes with sediment parameterization based on previous studies to describe the effects of bathymetry on sediment transport in the Hudson using ROMS. In another study with multiple classes, Ralston et al., (2013) used three non-cohesive classes to study sediment dynamics along intertidal flats in the Skagit Bay using FVCOM with the parameterization derived from available observations and literature values.

The aim of this paper is to validate an unstructured grid sediment model coupled to SELFE through a combination of idealized test cases (barotropic open channel, barotropic trench migration, and baroclinic tidally driven estuary) and a realistic application to an energetic estuary. The idealized tests are drawn from literature, and are designed to assess model skill at representing essential processes: suspended sediment transport, erosion and deposition, bed load transport, and morphological evolution. Model sensitivity to hydrodynamic and sediment parameterizations are described and optimal results are qualitatively compared against previous work and available analytical, semi-analytical, or laboratory results. Field observations from endurance stations and shipborne instrumentation in Columbia River estuary, USA are used to assess model skill in representing observed sediment dynamics in the complex and energetic Columbia River estuary. To facilitate future model inter-comparison and to promote the improvement in skill of sediment models, the tests and data are publically available as a benchmark (Lopez & Baptista, 2016).

## 2. Methods

### 2.1. Hydrodynamics model

SELFE (Zhang & Baptista, 2008) solves the Reynolds-averaged Navier–Stokes equations using both hydrostatic and Boussinesq assumptions. The governing equations are solved in a semi-implicit finite element ($P_1$–$P_{NC}$) framework using a combination of numerical methods. The advection of momentum is solved with a semi-Lagrangian method following Casulli & Cheng (1992). Scalar transport is solved using either upwind or total variation diminishing (TVD) Eulerian finite volume methods. Beyond the intrinsic differences between upwind and TVD, in SELFE the upwind scheme includes an implicit calculation of vertical flux, whereas TVD utilizes an explicit calculation resulting in a much slower time to solution. Comparisons of upwind and TVD transport schemes reveal minor differences in model skill of temperature and salinity in the Columbia River estuary. Because of the minor differences in skill and large differences in computational cost, we chose to use the much faster upwind scheme. Governing equations are closed by the general length scale (GLS) equations (Umlauf & Burchard, 2005) implemented in either a native SELFE implementation or by on-line coupling the GOTM library. The domain is discretized using a triangular, unstructured mesh in the horizontal similar to a hybrid CD grid and a hybrid Z- and S-level approach in the vertical.

In this paper, we discuss the implications of two distinct treatments for the solution of the momentum equation at the bottom boundary on represented sediment dynamics. As is common in coastal hydrodynamic models, SELFE uses a bottom boundary condition where the internal Reynolds stress is balanced with the stress from bottom friction

$$\nu \frac{\partial \boldsymbol{u}}{\partial z} = \boldsymbol{\tau_b} \tag{1}$$

where $\nu$ is the vertical eddy viscosity, $u$ is the velocity, $z$ is the vertical coordinate, and $\tau_b$ is the bottom stress. Assuming a turbulent boundary layer, a logarithmic velocity profile in the bottom boundary layer, and using turbulence closure theory to find the eddy viscosity results in a constant Reynolds stress in the bottom boundary layer:

$$\nu \frac{\partial \boldsymbol{u}}{\partial z} = \frac{\kappa_0}{ln(\delta_b/z_o)} \sqrt{C_D} |\boldsymbol{u_b}| \boldsymbol{u_b} \tag{2}$$

where $C_d$ is the drag coefficient, $z_0$ is the bottom roughness, $\kappa_0$ is the von Karman, $\delta_b$ is the thickness of the computational cell, and $\boldsymbol{u_b}$ is the bottom velocity (Zhang & Baptista, 2008). Specifically, $\boldsymbol{u_b}$ is taken to be the velocity at the top of the bottommost computational cell. Traditionally in SELFE, the discretized momentum equation was solved from the free surface to the top of the bottommost computational cell with the bottom node assigned a velocity of 0 to be consistent with a log layer adhering to the law of the wall. A new implementation, starting with version 4.0 of SELFE, solves the momentum equation from the surface to the bottom node to be consistent with the finite element formulation resulting in a non-zero velocity at the bottom node and an improved representation of the bottom boundary layer. The two implementations produce distinct estimates of $\boldsymbol{u_b}$ used in Eq. (2) resulting in distinct representations of bottom stress and shear. The implications of the new bottom boundary treatment of momentum for sediment modelling are discussed in idealized test cases. For convenience in differentiation, we refer to the traditional implementation as “no-slip” and the newer treatment as “slip” recognizing that formally both treatments are partial slip conditions.

### 2.2. Sediment model

The sediment model evaluated here is derived from the Community Sediment Transport Model (CSTM) (Warner et al., 2008). The non-cohesive classes, bed property changes, and bed morphology from the CSTM model were ported by Pinto et al., (2012) to work with the unstructured grids and methods used in SELFE. The model used here is algorithmically similar to Pinto et al., (2012), but was substantially refactored to align more closely with the original CSTM implementation. Minor implementation changes to improve stability including limiting slopes and increasing checks for numerically undefined numbers were required for the model to work in the Columbia River domain.

The sediment model solves for the time evolution of suspended sediments in three-dimensions and morphological changes. Specifically, the model calculates the vertical settling, bed load transport, and interactions with the bed through erosion and deposition for a user-defined number of non-cohesive classes. Suspended sediment concentrations are calculated by solving the advection-diffusion equation with additional terms for settling velocity and horizontal velocity

$$\frac{\partial \boldsymbol{C_n}}{\partial t} + \boldsymbol{u}\frac{\partial \boldsymbol{C_n}}{\partial x} + \boldsymbol{v}\frac{\partial \boldsymbol{C_n}}{\partial y} + \boldsymbol{w}\frac{\partial \boldsymbol{C_n}}{\partial z} = \frac{\partial}{\partial z}\left(\kappa \frac{\partial \boldsymbol{C_n}}{\partial z}\right) + \boldsymbol{w_{s,n}}\frac{\partial \boldsymbol{C_n}}{\partial z} + \boldsymbol{F_h} \tag{3}$$

where $C_n$ is the sediment concentration of class $n$, ($u$, $v$, $w$) are the directional velocity components, $\kappa$ is the eddy diffusivity, $w_{s,n}$ is the settling velocity of class $n$, and $F_h$ is the horizontal diffusion. Eq. (3) is solved using either the upwind or TVD transport schemes in SELFE (Zhang & Baptista, 2008). The vertical movement of sediment is handled using a hybrid WENO-PPM semi-Lagrangian method (Warner et al., 2008). Multiple bed layers are supported and erosional flux is calculated using the method outlined by Harris & Wiberg (2001). Specifically, the depositional flux, $D_n$, is calculated using

$$\boldsymbol{D_n} = \boldsymbol{w_{s,n}} \cdot \boldsymbol{C_b} \tag{4}$$

where $w_{s,\,n}$ is the settling velocity for sediment class $n$ and $C_b$ is the total sediment concentration in the bottom cell. The erosional flux for sediment class $n$, $E_n$, is defined as

$$\boldsymbol{E_n} = \begin{cases} \boldsymbol{E_{0,n}(1-p)f_p\left(\frac{\tau_{sf}}{\tau_{cr,n}}-1\right)}, & if\ \boldsymbol{\tau_{sf} > \tau_{cr,n}} \\ 0, & otherwise \end{cases} \tag{5}$$

where $E_{0,\,n}$ is the bed erodibility constant, $p$ is the porosity of the top layer of the sediment, $f_p$ is the volumetric fraction, $\tau_{sf}$ is the bed shear stress, $\tau_{cr,\,n}$ is the critical shear stress, $d_{50,\,n}$ is the median sediment diameter, $\rho_{s,\,n}$ is the density of the sediment, and $\rho_w$ is the density of the water. Bed load calculations use the formulation of either Meyer-Peter & Müller (1948) or van Rijn et al., (2007). Updates to bathymetry resulting from erosion, deposition, and bed load, the Exner equation, are calculated using the SAND2D bottom update module (Fortunato & Oliveira, 2004). This module uses a finite volume method where the sediment flux is conserved over the cells neighboring a node center using a forward Euler time-stepping scheme. The sediment module is also two-way coupled to the hydrodynamics of SELFE through the equation of state

$$\boldsymbol{\rho} = \boldsymbol{\rho_o} + \sum_{n=1}^{N} \frac{\boldsymbol{C_n}}{\boldsymbol{\rho_{s,n}}}(\boldsymbol{\rho_{s,n}} - \boldsymbol{\rho_w}) \tag{6}$$

where the new density $\rho$ includes densities of water and each sediment class weighted by their respective concentrations.

### 2.3. Model skill

As is common practice in applied sediment modeling, an important part of the skill assessment in this paper is qualitative. However, we also explore quantitative metrics that are commonly used in circulation modeling: root mean square error (RMSE), Willmott Score (WS), Murphy Score (MS), correlation coefficient (Corr), and bias.

The root mean square error (RMSE) is defined as,

$$\boldsymbol{RMSE} = \sqrt{\langle(\boldsymbol{m}-\boldsymbol{o})^2\rangle} \tag{7}$$

where $m = m_{i_i=1}^{n}$ are the modeled time series, $o = o_{i_i=1}^{n}$ are the observed times series, and • indicates the average over the series. The primary advantage of using RMSE results from the intuitive interpretation because the metric and measured values sharing the same units. A disadvantage of using RMSE is the large weight outliers impart on the metric and that it does not provide a means to compare variables measured in different units.

In contrast, the Willmott score (WS) allows comparison between variables because it is non-dimensional (Willmott, 1981). The WS is defined as

$$\boldsymbol{WS} = 1 - \frac{\langle(\boldsymbol{m}-\boldsymbol{o})^2\rangle}{\langle(|\boldsymbol{m}-\langle\boldsymbol{o}\rangle| + |\boldsymbol{o}-\langle\boldsymbol{o}\rangle|)^2\rangle} \tag{8}$$

A frequent criticism of the WS is the yielding of high skill scores for unrelated time series (Ralston et al., 2010).

An alternative skill metric that is not as susceptible to outliers, is non-dimensional, and allows for comparisons between units is the Murphy Score (MS),

$$\boldsymbol{MS} = 1 - \frac{\langle(\boldsymbol{m}-\boldsymbol{o})^2\rangle}{\langle(\boldsymbol{m_r}-\boldsymbol{o})^2\rangle} \tag{9}$$

where $m_r$ is the reference model that is compared against. A Murphy Score of 1 indicates a perfect model, 0 (zero) indicates that the model is equivalent to the reference model, and a negative score indicates skill worse than the reference. In this study, we typically use the mean of the observations as the reference model. However, for the trench migration test in Section 3.2 the reference model is the initial depth, and, following common nomenclature in the morphological literature (Sutherland et al., 2004), we refer in that case to the Murphy Score as the Brier Skill Score (BSS).

Finally, we also consider both correlation coefficient and bias for comprehensive purposes. The correlation coefficient, *Corr*, is a measure of linear correlation between two signals defined as

$$\boldsymbol{Corr} = \frac{\boldsymbol{COV(m,o)}}{\boldsymbol{\sigma_m\sigma_o}} \tag{10}$$

where COV($m$, $o$) is the covariance of model results $m$ and observations $o$ and their respective standard deviations are denoted by $\sigma_m$ and $\sigma_o$. The bias, is simply the mean difference between the model results and observations.

**Table 1**
Model parameters for open channel test.

| Parameter | Variables | Values |
|---|---|---|
| H-Grid | # nodes, # elems | 1111, 2000 |
| V-Grid | # S-levels | 21 |
| V-Grid | $H_c$, $\theta_b$, $\theta_f$ | 5.0, 1.0, 3.0 |
| Time step | dt [s] | 90 |
| Bottom roughness | $Z_{ob}$ [m] | 0.0053 |
| Initial density profile | [dp/dz] | 0 |
| Simulation length | [days] | 1 |
| Settling velocity | $w_s$ [mm/s] | 1 |
| Erosion rate | $E_o$ [kg/m$^2$/s] | $5\times10^{-5}$ |
| Critical stress | $\tau_{ce}$ [N/m2] | 0.05 |
| Porosity | $\Phi$ | 0.9 |
| Bed slope | $S_o$ | $4\times10^{-5}$ |
| Horizontal boundary condition | $\bar{u}$ [m/s] | 1 |

## 3. Idealized tests

### 3.1. Transport: steady open channel

This test evaluates the simulated transport of suspended sediment in an unstratified open channel and has been studied previously in Warner et al., (2008) and Pinto et al., (2012). The domain is a long open channel ($L$ = 10,000 m, $W$ = 1000 m, $H$ = 10 m) with a constant slope of $4\times10^{-5}$ m$^{-1}$. The boundary conditions consist of a fixed depth of 10 m imposed at the downstream end and a logarithmic velocity profile applied at the upstream boundary with a depth-averaged velocity of 1 m s$^{-1}$. The horizontal grid consists of 2000 elements and 1111 nodes, and 21 S-levels ($\theta_b$ = 1 and $\theta_f$ = 3) were used in the vertical. Both the SELFE and GOTM implementations of the GLS equations were tested to evaluate the effects of turbulence closure on the solution. Specifically, from the native SELFE GLS implementation we use *k-kl*, *k-ε*, and *k-ω* with the Kantha–Clayson stability function and *k-ε* and *k-ω* with the Canuto-A stability function from the GOTM library (Table 1). Strict direct comparisons between SELFE and GOTM implementations of the GLS equations are not possible for any specific closure model. The SELFE implementation does not have an option for the Canuto-A stability function, and GOTM would not converge to a solution when using Kantha–Clayson. Nevertheless, the selected turbulence closure models demonstrate important differences between the GLS implementation in GOTM and SELFE.

We compare the effects of the selection of the turbulence closure model and bottom boundary treatment on eddy diffusivity, turbulent kinetic energy (TKE), suspended sediment concentrations (SSC) and velocity profiles against semi-analytical and analytical solutions. (J. Paul Rinehimer, personal communication; see Appendix). The analytical solution assumes a Prandlt number of 0.8, a logarithmic velocity profile, a no-slip bottom boundary treatment, a Rouse SSC profile, and setting the free parameter $z_0$ to 0.0053 m to match the numerical experiments. The numerical semi-analytical solution is obtained from the numerical model

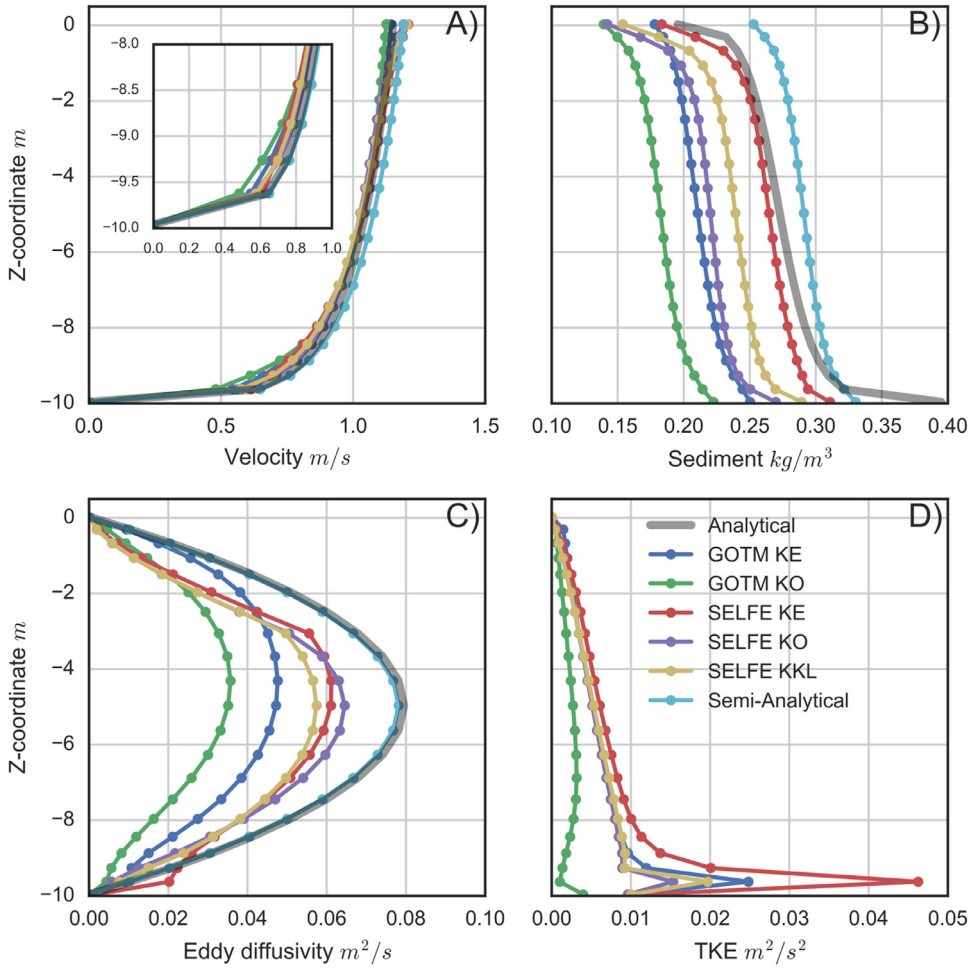


**Fig. 1.** Profiles of model results from open channel case with a no slip bottom boundary condition. Velocity (A), suspended sediment (B), eddy diffusivity (C), and TKE (D).

by imposing a parabolic eddy viscosity, $K_M$, and eddy diffusivity, $K_H$, instead of using a GLS turbulence closure model. The semi-analytical eddy viscosity and eddy diffusivity apply the same assumptions used in the calculations of the analytical solution.

Fig. 1 shows the results using the "no-slip" bottom boundary described in Section 2.1. All turbulence closures capture the analytical solution of velocity well, but underestimate near-bed velocities (Panel A). The SELFE implemented closures tend to underestimate velocity. The semi-analytical solution uniquely overestimates velocity throughout the water column compared to the analytical solution. The eddy diffusivity (Panel C) is underestimated for all closures, consistent with the findings of Warner et al., (2008) and Pinto et al., (2012). The native SELFE implementation of the GLS produces eddy diffusivity profiles distinctively skewed near the surface ($k$-$\varepsilon$ and $k$-$\omega$) and bottom ($k$-$\varepsilon$), whereas the GOTM closures produce smoother, non-symmetric profiles. Profiles for TKE (Panel D) feature large spikes one level above the bottom for all closures, but are amplified for SELFE implemented closures. SSC profiles (Panel B) are underestimated compared to the analytical and semi-analytical solutions, as found in previous studies (Pinto et al., 2012; Warner et al., 2008). SSC profiles result from a balance of the sediment settling velocity and the upward velocity from the eddy diffusivity implicating the underprediction of erosion and eddy diffusivity in the resulting in the underestimate of SSC.

For contrast, Fig. 2 shows results using the "slip" bottom boundary treatment. As was the case with the "no-slip" treatment, velocity profiles are well represented by all closures (Panel A), with the semi-analytical solution producing distinctive overestimations. However, all closures overestimate near-bottom velocities and most underestimate surface velocities when used with the "slip" bottom boundary. All closures again underestimate eddy diffusivity (Panel C), leading in aggregate to lower values than in the "no-slip" case. The convex shape near-the surface in the SELFE closures are still present, but are less severe and the near bed spikes are absent. Also, all profiles are now more symmetrical and thus, in that sense, closer to the analytical solution. The $k$-$\varepsilon$ closures produce the largest diffusivities, with the SELFE native implementation leading to the largest maximum value, but the GOTM implementation most closely aligns with the analytical solution. For TKE (Panel D), the artificial near-bottom spikes are eliminated for GOTM closures and substantially reduced for SELFE implementations. Estimates of SSC (Panel B) are lower than those predicted in the "no-slip" case, which is attributed to the elimination or reduction of artificial near-bed TKE spikes.

Comparisons of bottom shear stress (used to calculate erosion), erosion rate, eddy diffusivity, and SSC are shown in Table 2. These results show that skill of SSC requires accurate predictions of eddy diffusivity and is less sensitive to deviations in bottom shear stress. The SELFE GLS implementations produce higher values of eddy diffusivity and, therefore, SSC, but at the cost of producing physically questionable profiles of eddy diffusivity and TKE. In contrast, the GOTM implementation predicts lower values of eddy diffusivity with smooth profiles that better match the shape of the semi-analytical and analytical solution. Given these tradeoffs, we believe that the combined used of the "slip" bottom boundary and GOTM for turbulence closure is the superior choice. We also

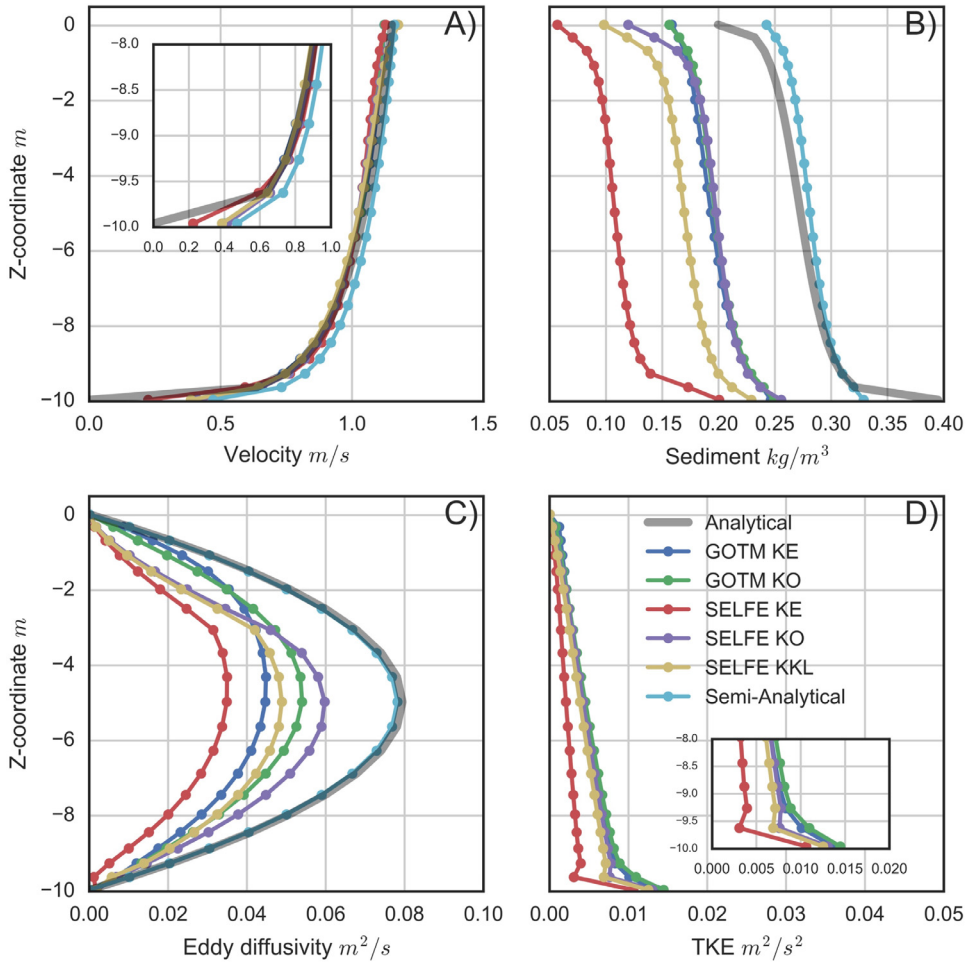


**Fig. 2.** Profiles of model results from the open channel case with a slip bottom boundary condition. Velocity (A), suspended sediment (B), eddy diffusivity (C), and TKE (D).

**Table 2**
Description of turbulence closure models used for open channel test case and relevant values for bottom shear stress ($\tau_b$ [Pa]), erosional flux (kg/m$^2$/s), eddy diffusivity (Kh [m$^2$/s]), and suspended sediment concentrations (SSC [kg/m$^3$]) taken at one vertical level above the bed.

| BBL | Turbulence model | Stability function | Tb | Erosion | Kh | SSC |
|---|---|---|---|---|---|---|
| No-slip | Calculated Kh & Km | – | 3.9062 | 3.856-e04 | 0.0104 | 0.314 |
| No-slip | GOTM *k-ε* | Canuto-A | 2.6797 | 2.630e-04 | 0.0092 | 0.244 |
| No-slip | GOTM *k-O* | Canuto-A | 2.0795 | 2.029e-04 | 0.0044 | 0.214 |
| No-slip | SELFE *k-ε* | Kantha–Clayson | 3.3842 | 3.334e-04 | 0.0202 | 0.294 |
| No-slip | SELFE *k-O* | Kantha–Clayson | 2.8742 | 2.824e-04 | 0.0057 | 0.250 |
| No-slip | SELFE *k-kl* | Kantha–Clayson | 2.9958 | 2.946e-04 | 0.0076 | 0.269 |
| No-slip | Imposed Kh & Km | – | 3.7955 | 3.745e-04 | 0.0102 | 0.321 |
| Slip | GOTM *k-ε* | Canuto-A | 3.6835 | 3.634e-04 | 0.0069 | 0.239 |
| Slip | GOTM *k-O* | Canuto-A | 3.9016 | 3.852e-04 | 0.0073 | 0.240 |
| Slip | SELFE *k-ε* | Kantha–Clayson | 3.1728 | 3.123e-04 | 0.0011 | 0.173 |
| Slip | SELFE *k-O* | Kantha–Clayson | 3.8474 | 3.847e-04 | 0.0069 | 0.237 |
| Slip | SELFE *k-kl* | Kantha–Clayson | 3.7432 | 3.693e-04 | 0.0059 | 0.212 |
| Slip | Imposed Kh & Km | – | 4.8309 | 4.781e-04 | 0.0102 | 0.320 |

note that this test highlights the inherent sensitivity of sediment models to model parameterization and numerical implementation, even in highly constrained tests.

### 3.2. Bed dynamics: trench migration

This test is used to validate the implementation of suspended sediment, bed load, and morphology algorithms and is based on the flume experiments described in (van Rijn, 1993). The domain is an open channel ($L$ = 30 m, $W$ = 5 m) with a constant slope of $4.0 \times 10^{-4}$ m$^{-1}$ featuring a trench cut into the bed. The bed and suspended sediments are comprised of a single non-cohesive class $D_{50}$ = 0.16 mm with the settling velocity derived from the Stokes settling velocity and imposed as a constant value ($w_s$ = 11 mm s$^{-1}$). The upstream hydrodynamic boundary condition consists of a constant velocity and depth ($h_0$ = 0.39 m, $u_0$ = 0.51 m s$^{-1}$) and suspended sediments are supplied upstream at a constant concentration of 0.14 kg m$^{-3}$ to ameliorate erosion. The model hydrodynamics and suspended sediment are spun up with a fixed bed until the currents and SSC reach a steady state after ~25 min. The morphological algorithms are then enabled and the simulation proceeds for 15 h more. A global time step of 0.375 s, correspond-

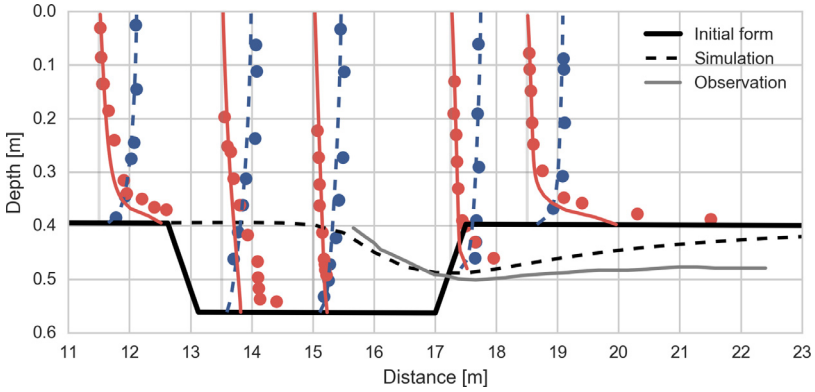


**Fig. 3.** Velocity (dashed blue) and suspended sediment (solid red) profiles comparing observations (circle markers) with model results (lines). Also depicted are measured and calculated bathymetric profiles of the migrating trench test case. (For interpretation of the references to color in this figure legend, the reader is referred to the web version of this article).

**Table 3**
Model parameters for trench migration test.

| Parameter | Variables | Values |
|---|---|---|
| H-Grid | # nodes, # elems | 1205, 1920 |
| V-Grid | # S-levels | 30 |
| V-Grid | $H_c$, $\theta_b$, $\theta_f$ | 7.0, 1.0, 10.0 |
| Time step | dt [s] | 0.375 |
| Bottom roughness | $Z_{ob}$ [m] | 0.00'5 |
| Initial density profile | [dp/dz] | 0 |
| Simulation length | [h] | 15 |
| Settling velocity | $w_s$ [mm/s] | 11 |
| Erosion rate | $E_o$ [kg/m$^2$/s] | $0.7 \times 10^{-2}$ |
| Critical stress | $\tau_{ce}$ [N/m2] | 0.11 |
| Porosity | $\Phi$ | 0.4 |
| Bed slope | $S_o$ | $4 \times 10^{-4}$ |
| Horizontal boundary condition | $\bar{u}$ [m/s] | 0.51 |

ing to a CFL (Courant–Friedrichs–Lewy) number of 1.5, was used based on sensitivity analysis (not shown) and is 7.5 times longer than the used in Pinto et al., (2012). The parameters were derived from sensitivity analysis to match observations of velocity and suspended sediment as described in van Rijn (1986) and to alleviate bed erosion upstream of the trench. We ultimately retained an erosion rate of $0.7 \times 10^{-2}$ kg m$^{-2}$ s$^{-1}$, compared to the rate of $1.6 \times 10^{-2}$kg m$^{-2}$ s$^{-1}$ used in Pinto et al., (2012), which produced excessive erosion and trench migration in our simulations. A summary of the model parameters is provided in Table 3.

Comparisons of profiles of suspended sediment and velocity between estimates of laboratory observations (markers, van Rijn (1986)) and model results (lines) are shown in Fig. 3. Model profiles of velocity match observations most closely outside of the trench where a clear logarithmic profile is found in both the observations and model results. Stations within the trench show both slight overprediction and underprediction of velocity within a single profile, but are close to observations in magnitude. Profiles of SSC align with observations but have worse skill than the velocity profiles. In particular, the modeled SSC profiles underestimate concentrations near the bed. The underprediction of SSC is likely due to do a combination of underpredicted erosion and eddy diffusivity, as seen in the open channel case. Increasing the erosion rate yields increased SSC but produces excessive erosion and trench migration. The velocity and SSC skill appears to lag those produced by ROMS (Warner et al., 2008) and Delft3D (Lesser et al., 2004), but are similar to the results in Pinto et al., (2012). The trench migration is very similar to observations and aligns with the previously published results of Pinto et al., (2012) and Warner et al., (2008) despite using different parameters for erosion rate and critical stress. Skill scores for the trench migration case

**Table 4**
Model skill for predicted bed depth in the trench migration case.

| Variable | Bias | Corr | WS | BSS | RMSE |
|---|---|---|---|---|---|
| Bed depth | −0.02 | 0.41 | 0.54 | 0.84 | 0.02 |

are shown in Table 4. The difference in the predicted final position of the trench results from underprediction of SSC and likely from underprediction of bedload transport.

Calibration simulations (not shown) confirm that the model is very sensitive to erosion rate parameterizations and must be carefully tuned to ensure that the SSC profiles align with observations. As in the open channel case in Section 3.1, this highlights the inherent uncertainty in sediment models in even highly constrained cases. However, the trench and open channel cases differ in some important respects. In particular, the calculated TKE in the upstream section of the trench does not exhibit the near-bed spike as seen in the open channel case, regardless of whether GOTM or SELFE are used for turbulence closure. Additionally, the GOTM eddy diffusivity deviates from a smooth profile near the surface, whereas the SELFE profile is very similar to that found in the open channel case (Fig. 4). This likely results from the much higher vertical resolution used in this shallow test case (30 vertical levels in 0.4 m) compared to the open channel case (21 vertical levels in 10 m) which is more representative of the resolution used in realistic scenarios.

Another difference is that, unlike in the open channel case (Section 3.1), trench migration results are largely insensitive to the selection of turbulence closure, but quite sensitive to the bottom boundary treatment (results not shown). This is because of the dominance of bed dynamics in the trench case whereas the open channel case lacks morphological evolution. Because the erosional flux is determined by near-bed velocities, changes in the treatment of the bottom boundary layer produce proportional changes in the bed evolution. This suggests that accurate simulation of near-bed velocities and bed properties are more important than turbulence closure in systems dominated by bed interactions.

### 3.3. ETM dynamics: idealized estuary

This test is used to assess the ability of the sediment model to represent processes associated with the generation of an estuarine turbidity maximum (ETM). The test is derived from Burchard & Baumert (1998) and Warner et al., (2007), who used variations of it to assess the importance of ETM related processes and to

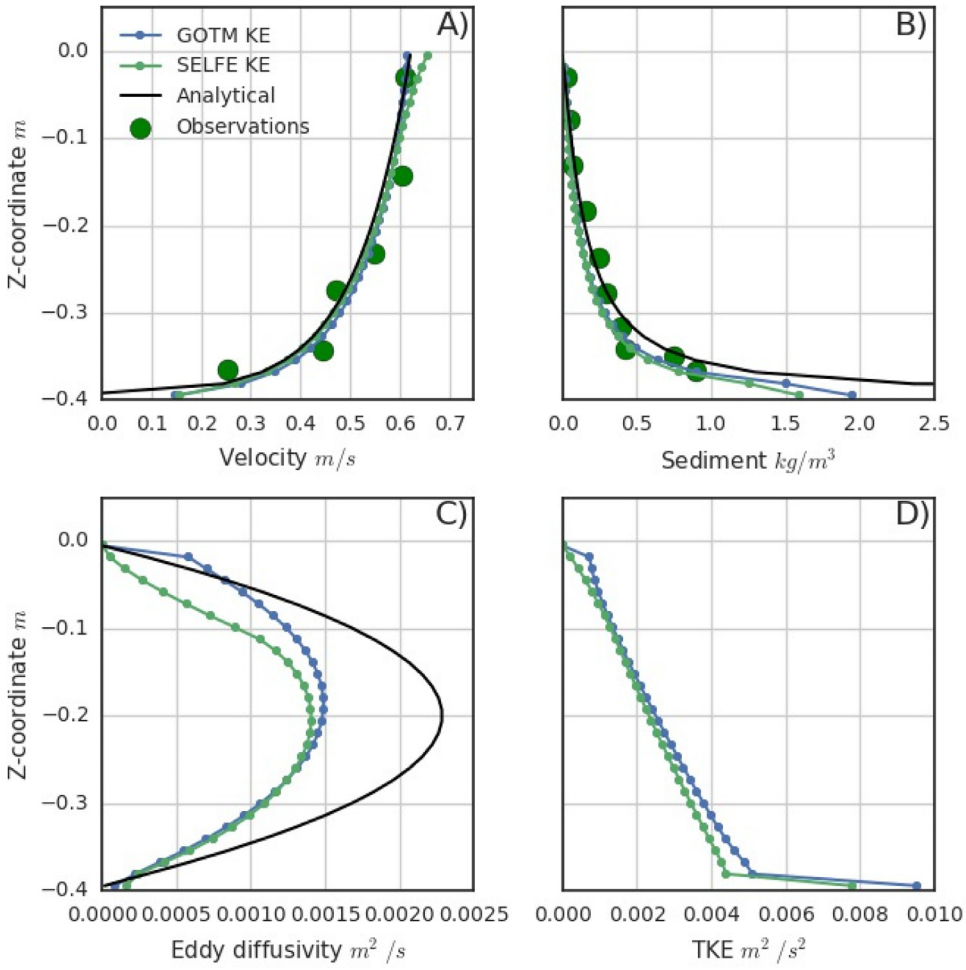


**Fig. 4.** Profiles of model results from the trench migration case with a slip bottom boundary condition taken at the first observation station in the upstream portion of the domain at the end of the spin-up period. Results show for GOTM (blue) and SELFE (green) implementations of GLS equations. Velocity (A), suspended sediment (B), eddy diffusivity (C), and TKE (D). (For interpretation of the references to color in this figure legend, the reader is referred to the web version of this article).

describe those processes over tidal time scales. The domain is effectively a two-dimensional open channel 100 km in length and 200 m in width. The domain features a constant sloping bottom starting with a 5 m depth at the upstream boundary and ending with a 10 m depth at the downstream boundary. The ocean boundary is forced with a semi-diurnal displacement of the free surface with an amplitude of 0.4 m and a period of 12 h and the constant imposition of salinity at 30 PSU and temperature at 10 C. The upstream boundary is forced with a constant flux of 80 $m^3$ $s^{-1}$, salinity of 0 PSU, and temperature of 10 C. The hydrodynamics are allowed to spin-up for 14 days whereupon the initial conditions have been eliminated from the domain and a regular pattern of gravitational circulation has been established. We note that the solution to the problem is highly sensitive to the density forcing at the downstream boundary. Sensitivity tests (not shown) suggest that slight perturbations in the forcing results in both different spin-up period lengths and characteristics of the gravitational circulation patterns including salinity and SSC distribution.

Fig. 5 shows tidally averaged salinity, SSC, and along-along channel velocity. The predicted representation of the salt wedge and sediment concentrations are very similar to those described in Burchard & Baumert (1998) and Warner et al., (2007). Specifically, the distribution of sediment in the channel can be divided into three distinct areas corresponding to the well-mixed upstream fluvial section, a stratified bottom boundary layer corresponding to the salt wedge, and a surface layer above the salt wedge. The well-mixed upstream section features residual downstream velocity and low SSC that steadily increases in proximity to the salt-wedge and the region of convergent currents. The highest velocities in the domain are found in the surface layer above the salt wedge where they are oriented downstream and contain the lowest SSC because the sediment tends to settle through the pycnocline into the salt wedge. Within the salt wedge, the residual velocities are oriented upstream carrying the highest concentrations of SSC in the system. Of particular interest, a localized region of elevated SSC occurs near the toe of the salt wedge, the classical ETM, due to trapping of sediment by the convergent currents. Finally, the salt wedge region contains SSC above both the riverine and ocean end members sourced from a combination of sediment settling from the upper layer, erosion from the bed, and residual upstream transport.

While this test case lacks analytical solutions or reference observations, it remains a critical check of a model's ability to represent the coupled circulation and sediment dynamics required to generate elevated turbidity near the upstream limit of salt intrusion in estuaries. Qualitative comparisons with results described in literature (Burchard & Baumert, 1998; Warner et al., 2007) show that SELFE produces similar results for density, SSC dynamics, and magnitude and location of SSC peaks. These similarities suggest the model is capable of representing ETM dynamics, a common sedimentary feature in many tidally driven estuaries.

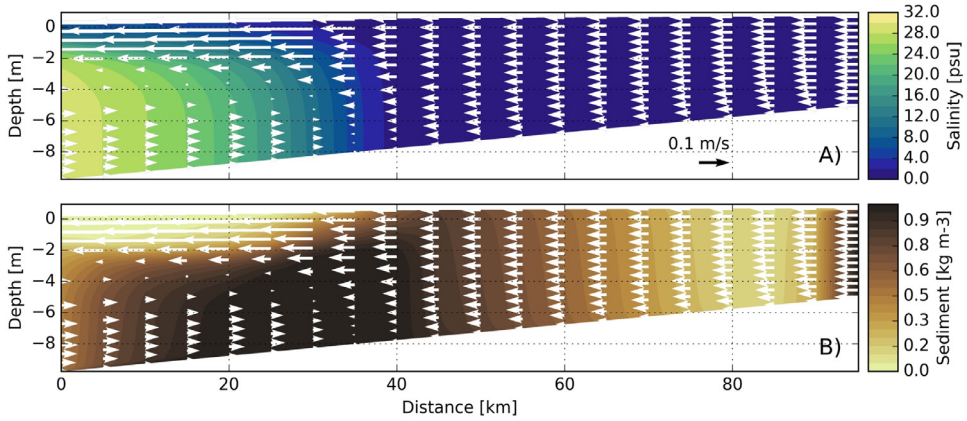


**Fig. 5.** Transects of tidally averaged salinity and suspended sediment concentrations in an idealized 2D channel. Velocity profiles are shown with grey arrows. Three distinct regions are found corresponding to: (1) a fresh, low SSC upstream section; (2) a brackish, low SSC region with downstream focused velocity above the pycnocline; (3) a saline, high SSC section with upstream focused velocity.

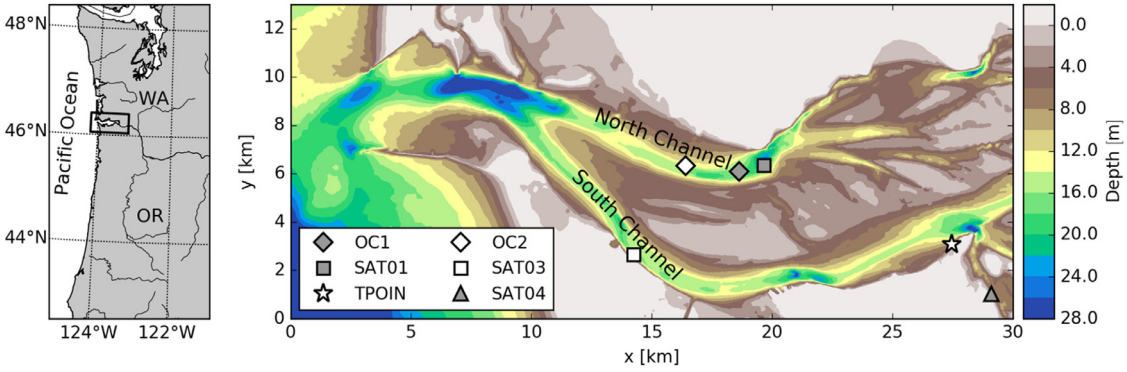


**Fig. 6.** Map of the Columbia River estuary with stations and anchorages where data was collected.

## 4. Columbia River benchmark

The Columbia River is the largest river to discharge into the North East Pacific Ocean. It has a mean discharge of 8000 $m^3\ s^{-1}$, with a minimum of ~3000 $m^3\ s^{-1}$ during dry autumnal months and over 15,000 $m^3\ s^{-1}$ during large spring freshets. The estuary has two main channels separated by broad intertidal shoals and is flanked by four lateral bays (Fig. 6). The South Channel receives the majority of the fluvial flux and is regularly dredged for navigation purposes. In contrast, the North Channel is not maintained for transport and receives the majority of the tidal prism (Chawla et al., 2008). The tides in this system are mixed, semi-diurnal with a tidal range that varies from ~2 m for the smallest neap tides to ~3.5 m during the largest spring tides.

### 4.1. Field observations

Two in-situ sensor networks provide nearly continuous observations for model-data comparisons (Fig. 6). From the tidal gauge network of the National Oceanic and Atmospheric Administration, we use time series of elevations from the Tongue Point, OR station along the South Channel. From the Center for Coastal Margin and Prediction interdisciplinary SATURN network (Baptista et al., 2015), we use temperature, salinity, and turbidity time series from stations SATURN-03 (in the South Channel) and SATURN-04 (in Cathlamet Bay).

In addition, we make model-data comparisons with a single-vessel research cruise that took place between October 25 and November 3, 2012, aimed at characterizing ETM dynamics (Sanford et al., 2015). The cruise's geographic scope was the North Channel with anchorages at OC1 and OC2 (Fig. 6). Vessel-based instrumentation included a boom mounted acoustic Doppler current profiler (ADCP), a conductivity temperature depth (CTD) package, a flow-through optical backscatter sensor (OBS), and the CMOP Winched Profiler (CMOP-WP). The CMOP-WP is a multi-instrument sensor package comprised of a Seabird SBE 37 CTD, WetLabs EcoPuck, a Sequoia LISST-1000X, Sea-bird $\mu$C and $\mu$T, and a Sontek acoustic Doppler velocimeter (ADV). Additional details about the CMOP-WP can be found in Kärnä et al., (2015). The CMOP-WP continuously profiled the water column for the duration of the cruises. Water samples were collected before, during, and after each passing of the ETM and were processed using the method described by Reed & Donovan (1994) using a modified Owen Tube to collected samples that were then filtered, dried, and weighed to determine the amount of suspended sediment. These data were combined with measurements of SSC from the USGS station at Beaver Army Terminal and turbidity measurements from the same instrument type at SATURN-05 (also located at Beaver Army Terminal) to create a predictive model of SSC from NTU measurements. A least squares fit of the observations (Fig. 7) yielded the relation

$$\mathbf{SSC} = 2.16 \cdot \mathbf{NTU}^{1.26} \tag{11}$$

where SSC is the estimated suspended sediment concentration and NTU is the observed turbidity from the optical instrument ($R^2 = 0.76$).

### 4.2. Model parameterizations

The application of SELFE to the Columbia River estuary benefits from the extensive prior history of sensitivity studies, model

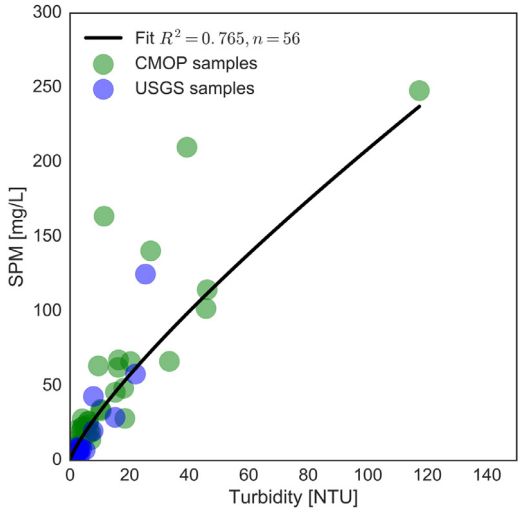


**Fig. 7.** Observations of suspended sediment concentrations and optical turbidity measurements with the least squares fit the log-transformed data.

parameterization, and validation for SELFE-based circulation simulations in that system. In particular, we use the same numerical choices and hydrodynamic parametrization for SELFE described in Kärnä et al., (2015). The numerical methods used for this application are the same as those described in Section 2.1. A second-order $k$-$\varepsilon$ model from GOTM is used for turbulence closure which has shown to maximize salinity retention in the estuary in sensitivity studies (not shown). An optimal global time step of 36 s was derived from sensitivity studies, with the time step for the transport equations sub-iterated to avoid CFL violations. River discharge and temperature boundary conditions are imposed at Beaver Army Terminal from observations (USGS #14,246,900). The top eight tidal constituents from a regional inverse model (Myers & Baptista, 2001) are imposed along the ocean boundary. Temperature, salinity, and sub-tidal elevations are imposed along the same boundary from Navy Coastal Ocean Model (NCOM) simulations (Barron et al., 2006). In a buffer region (50 km) near the ocean boundary, temperature and salinity fields are nudged toward NCOM values on a time scale of two days. Atmospheric boundary conditions of wind speed, air pressure, and radiative heat flux are forced from the NOAA/NCEP North American Mesoscale Forecast System (Rogers et al., 2009).

The horizontal mesh (56 K 2D nodes, 109 K 2D elements) covers the Columbia River estuary from Beaver Army Terminal 85 km upstream of the mouth through the continental shelf to 300 km off the coast from latitudes 39–50 N. The domain is highly resolved in the estuary and more coarsely represented in the plume and far-field ocean. The domain includes the river-to-shelf continuum to capture the effects of shelf-scale processes such as upwelling and plume dynamics on estuarine circulation. The flexibility provided by the unstructured mesh used by SELFE is ideally suited to represent fine structures within the estuary, the complicated coastline within and outside of the estuary, and the winding main channel to the first convenient boundary condition at Beaver Army Terminal. The vertical structure is resolved using 37 stretched S-levels ($H_c = 30$, $\theta_b = 0.7$, $\theta_f = 10$) in most of the domain with an additional 17 Z-levels in stretches deeper than 100 m. Bottom roughness is imposed with a uniform $Z_0$ of 0.0001 m, based on calibration runs to optimize model representation of salinity (Kärnä et al., 2015).

The sediment model is parameterized from a combination of observations, literature values, and a set of subsequent calibration simulations (not shown). We use four sediment classes with settling velocities of 0.05, 0.5, 2.0, and 10.0 mm $s^{-1}$ which are representative of the suspended sediment size classes found in the Columbia River estuary (Fain et al., 2001). These classes range from silts to fine sands with details related to median size and settling speed described in Table 5. The initial bed distributions are derived from literature descriptions of the system and are dominated by the sand size class because the bed is almost completely devoid of clay or fluid mud (Fox et al., 1984;Fain et al., 2001; Sherwood & Creager, 1990). The riverine boundary conditions for sediment concentrations are derived from a rating curve derived from water samples of suspended sediments at Beaver Army Terminal (USGS #14,246,900). Water samples of SSC and mean daily flow were log-transformed and fit using a least squares method following the methods described in Warrick (2015), yielding the relation

$$SSC = e^{-18.6} Q_r^{1.65} \tag{12}$$

where $Q_r$ is the river flux ($m^3$ $s^{-1}$) and $SSC$ is suspended sediment (mg $L^{-1}$) ($R^2 = 0.79$). The rating curve predicts SSC concentrations of 0.005–0.022 kg $m^{-3}$ for the modeled time period, comparing adequately with available observations of 0.01–0.02 kg $m^{-3}$. The ocean boundary conditions are derived from oceanic (>30 PSU) water samples collected during the cruise described in Section 4.1 and were imposed as a constant 0.005 kg $m^{-3}$. Erosion rate, critical shear stress, and porosity are all derived from literature values for similar size classes (Ralston et al., 2013; Warner et al., 2008) from systems with similarities in sediment composition and characteristics. Erosion rate and critical shear were then calibrated (not shown) using model skill at SATURN stations and anchorages OC1 and OC2 as the metric.

**Table 5**
Sediment model parameters used for simulations of the Columbia River estuary.

| Variable | Wash | Fine silt | Silt | Sand |
|---|---|---|---|---|
| Median diameter [mm] | 0.01 | 0.03 | 0.06 | 0.125 |
| Settling velocity [mm/s] | 0.05 | 0.05 | 2.0 | 10.0 |
| Erosion rate [kg/m2/s] | $1.0 \times 10^{-5}$ | $1.0 \times 10^{-4}$ | $1.0 \times 10^{-4}$ | $1.0 \times 10^{-3}$ |
| Critical stress [Pa] | 0.10 | 0.15 | 0.15 | 0.2 |
| Porosity | 0.65 | 0.60 | 0.55 | 0.50 |
| Bed initial conditions [%] | 0.05 | 0.10 | 0.10 | 0.75 |
| Boundary conditions [%] | 0.10 | 0.20 | 0.20 | 0.50 |

### 4.3. SATURN station comparisons

In this section, we compare model results to observations of temperature, salinity, and turbidity measurements at SATURN-03 and SATURN-04, and of elevation at Tongue Point, OR. Estimates of SSC are obtained from an empirical correlation (Eq. (11)) between water samples from research cruises and stations (USGS #14,246,900) and optical turbidity measurements (Fig. 7).

SATURN-03 is located in the South Channel approximately 23 km upstream of the mouth. Located within the extent of salinity intrusion, this station captures the estuary's strong variability in response to tidal and river forcing. The station is equipped with a pump-based system where water is collected at ports 2.4, 8.2, and 13 m below Mean Sea Level (MSL) in sequence, and piped to a single instrument package where salinity and turbidity are measured. In-water temperature sensors are collocated with each port.

Observations at this station show that the highest SSC occur during spring tides and the lowest during neap tides (Fig. 8). The correlation between tidal range and SSC is strongest near the bed and diminishes toward the surface where average SSC and the

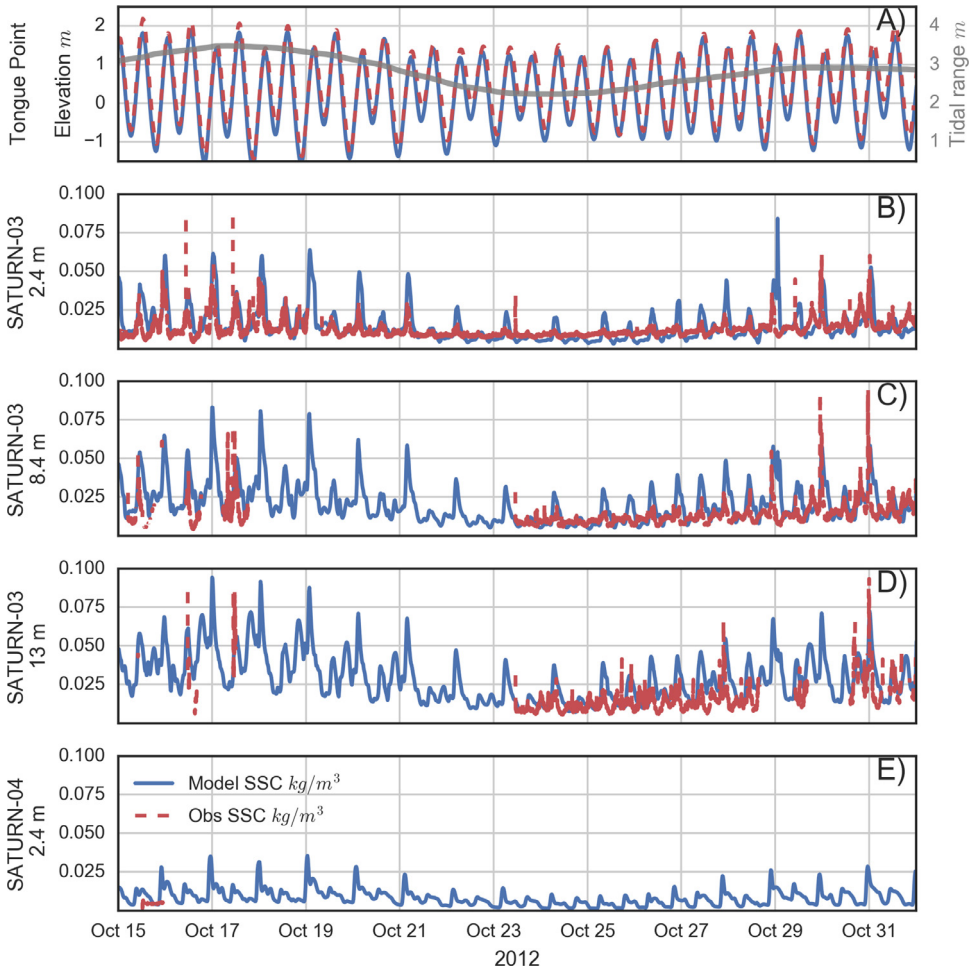


**Fig. 8.** The figure shows a comparison of predicted suspended sediment concentrations at SATURN stations at multiple depths compared against feature observations. Shown are model elevation (blue) and elevation (red) and tidal range (grey) observations from Tongue Point, Oregon (A), model (blue) and observations (red) of SSC at depths of 2.4 m (B), 8.4 m (C), and 13.0 m (D) at SATURN-03, and at 0.4 m depth at SATURN-04 (E). (For interpretation of the references to color in this figure legend, the reader is referred to the web version of this article).

tidal variability of SSC decrease. The observed SSC is also strongly correlated with semi-diurnal tidal patterns: the highest concentrations within a tidal day occur during the floods immediately following large ebbs. Model results qualitatively capture tidal day and tidal month patterns of variability as suggested by the average correlation coefficient for the station, Corr = 0.52 (Table 6). The average Willmott Score, WS = 0.64, suggests good skill, but the more rigorous Murphy Score indicates skill worse than the observed mean (MS = −0.91). The simulated tidally averaged SSC also reveal a correlation with tidal range, which observations for this time period also suggest.

SATURN-04 is located near the entrance of Cathlamet Bay south of the South Channel just upstream of Tongue Point. This station remains largely fresh throughout the year, but periodic pulses of brackish water are observed during periods of low and moderate river discharges. Structurally similar to SATURN-03, this station collects data at 0.3 m below the water surface and 8.6 m below MSL. Model skill for SATURN stations is summarized in Table 6.

Fouling of the turbidity sensor limited data availability during the targeted time period. Despite this, Fig. 8 shows that available measurements to provide context, offer a rough estimate of SSC, and to enable a rough assessment of the model skill in an unstratified region of the estuary. Model results are similar in magnitude to observations and suggest that SSC is lower at this station than at SATURN-03 or at the locations profiled by the CMOP-WP (Section 4.4). Model results also suggest reduced spring-neap variability compared to SATURN-03. The comparatively lower values of SSC observed and predicted by the model are consistent with SATURN-04 lying outside the ETM region.

**Table 6**
Model skill from *R/V Oceanus* anchorages OC1 and OC2 data collected by the Winched Profiler and SATURN-03 at 2.4 m (S), 8.2 m (M), and 13 m (B) depths.

| Site | Variable | Bias | Corr | WS | MS | RMSE |
|---|---|---|---|---|---|---|
| OC1 | Velocity | −0.13 | 0.95 | 0.96 | 0.77 | 0.37 |
| OC1 | Salt | −3.95 | 0.87 | 0.89 | 0.46 | 6.64 |
| OC1 | Temp | 0.17 | 0.69 | 0.69 | 0.25 | 0.35 |
| OC1 | SSC | 0.01 | 0.16 | 0.41 | −0.72 | 0.02 |
| OC2 | Velocity | −0.15 | 0.96 | 0.97 | 0.87 | 0.32 |
| OC2 | Salt | −1.20 | 0.92 | 0.95 | 0.80 | 4.59 |
| OC2 | Temp | 0.17 | 0.67 | 0.69 | 0.26 | 0.54 |
| OC2 | SSC | 0.02 | 0.69 | 0.57 | −4.06 | 0.02 |
| SATURN-03 S | Salt | −1.583 | 0.947 | 0.956 | 0.788 | 3.426 |
| SATURN-03 M | Salt | 0.054 | 0.961 | 0.979 | 0.912 | 2.386 |
| SATURN-03 B | Salt | −2.185 | 0.858 | 0.882 | 0.504 | 3.499 |
| SATURN-03 S | Temp | −0.116 | 0.735 | 0.844 | 0.434 | 0.510 |
| SATURN-03 M | Temp | −0.9097 | 0.711 | 0.830 | 0.452 | 0.503 |
| SATURN-03 B | Temp | 0.143 | 0.664 | 0.798 | 0.361 | 0.487 |
| SATURN-03 S | SSC | 0.002 | 0.537 | 0.664 | −1.042 | 0.008 |
| SATURN-03 M | SSC | 0.004 | 0.458 | 0.609 | −1.114 | 0.011 |
| SATURN-03 B | SSC | 0.007 | 0.554 | 0.646 | −0.808 | 0.012 |

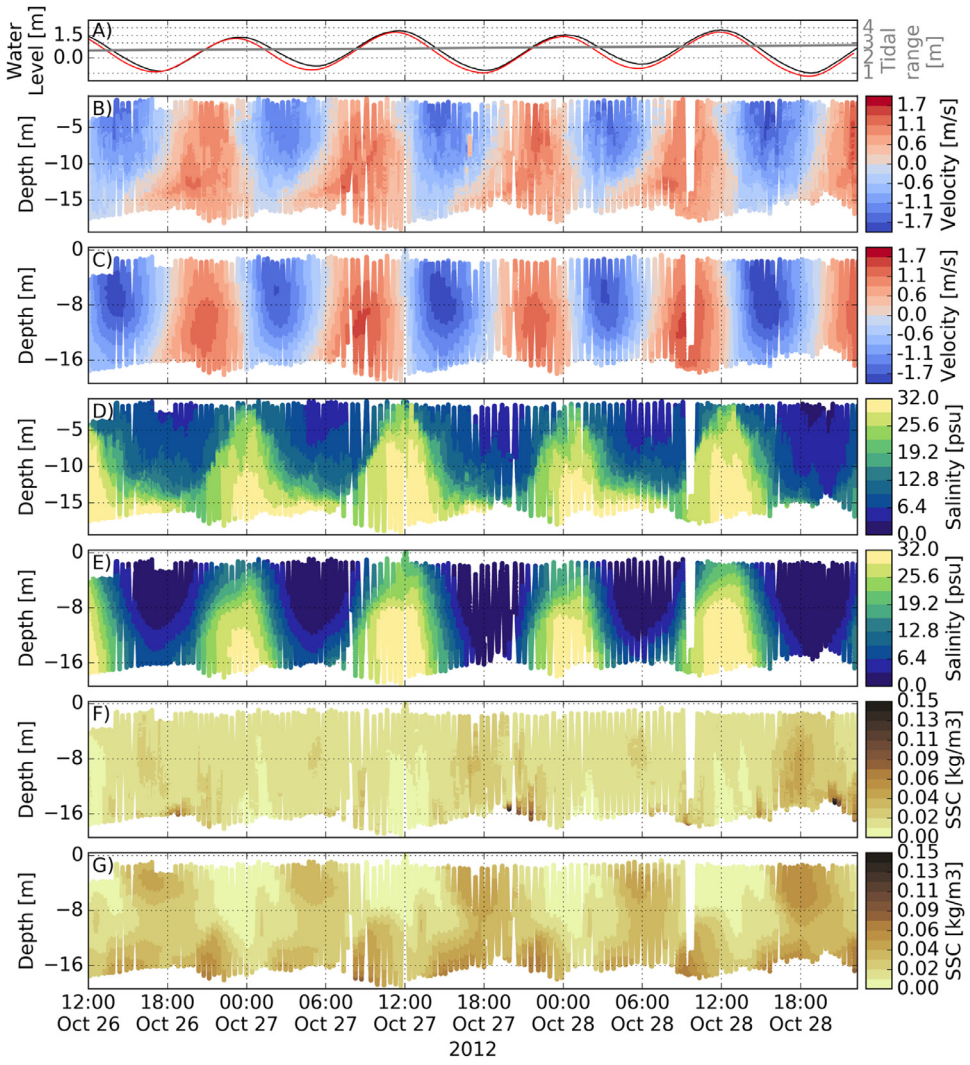


**Fig. 9.** Comparisons of observations and model results at anchorage OC1 from the Winched Profiler for water levels (A), stream-wise velocity (B), modeled stream-wise velocity (C), salinity (D), modeled salinity (E), SSC (F), and modeled SSC (G). The gray line in (A) is the tidal range for the observation period.

### 4.4. Winched profiler comparisons

Here we compare model results to the shipborne observations in the North Channel as captured by the CMOP-WP during the fall 2012 cruise (Fig. 6). Specifically, we compare temperature, salinity, velocity, and SSC values as measured by the CMOP-WP and model results using the statistical metrics described in Section 2.3 (Table 6).

#### 4.4.1. Flow field comparisons

The skill of the circulation model has been described in detail in Kärnä et al., (2015), but the pertinent points are summarized here for context. Model skill at OC1 (Fig. 9) and OC2 (Fig. 10) has been calculated separately and is summarized in Table 6. Model skill at OC1, during the transition from neap to spring tides, lags that at OC2, during spring tides, according to all skill metrics except for the MS. Qualitatively, the overprediction of SSC at OC2 (MS = −4.06, WS = 0.57) makes the model results appear to have less skill than those at OC1 (MS = −0.72, WS = 0.41).

At OC1 the shape of the salt wedge and salinity distribution of the major floods is well represented by the model (Fig. 9). In both the model and observations, salinities associated with the salt wedge over 20 PSU are present in the surface layer and salinities over 30 PSU are found in the lower layer. Model skill for all fields diminishes during ebbs, when the model underestimates the retention of salt near the bed, the presence of two distinct layers, and the setup of exchange flow as documented in Kärnä et al., (2015). The lack of a two-layer representation at OC1 during ebbs results in an overestimate of seaward velocities throughout the water column, but is most prominent near the bed and is reflected in the bias (−0.13 m/s). Nevertheless, the model captures the tidal variability of along-channel velocities according to all skill metrics (MS = 0.77, WS = 0.96). Model skill of salinity (MS = 0.46, WS = 0.89) lags that of velocity due to the underprediction of salinity during ebbs.

At OC2 the model skill is highest during flood and degrades during major ebbs, as was the case at OC1 (Fig. 10). For example, the model shows the salt wedge being advected downstream of the station during the major ebb between 10:00 and 18:00 on October 29 leaving the water column nearly fresh. In contrast, observations show that the salt wedge remained at OC2 and that the water column remained stratified. The lack of salinity retention is reflected in the bias (−1.2 PSU), but is not apparent in other metrics (MS = 0.80, WS = 0.95). In both the observations and model results, the fastest upstream velocities are localized to a region within the pycnocline during minor floods but produce

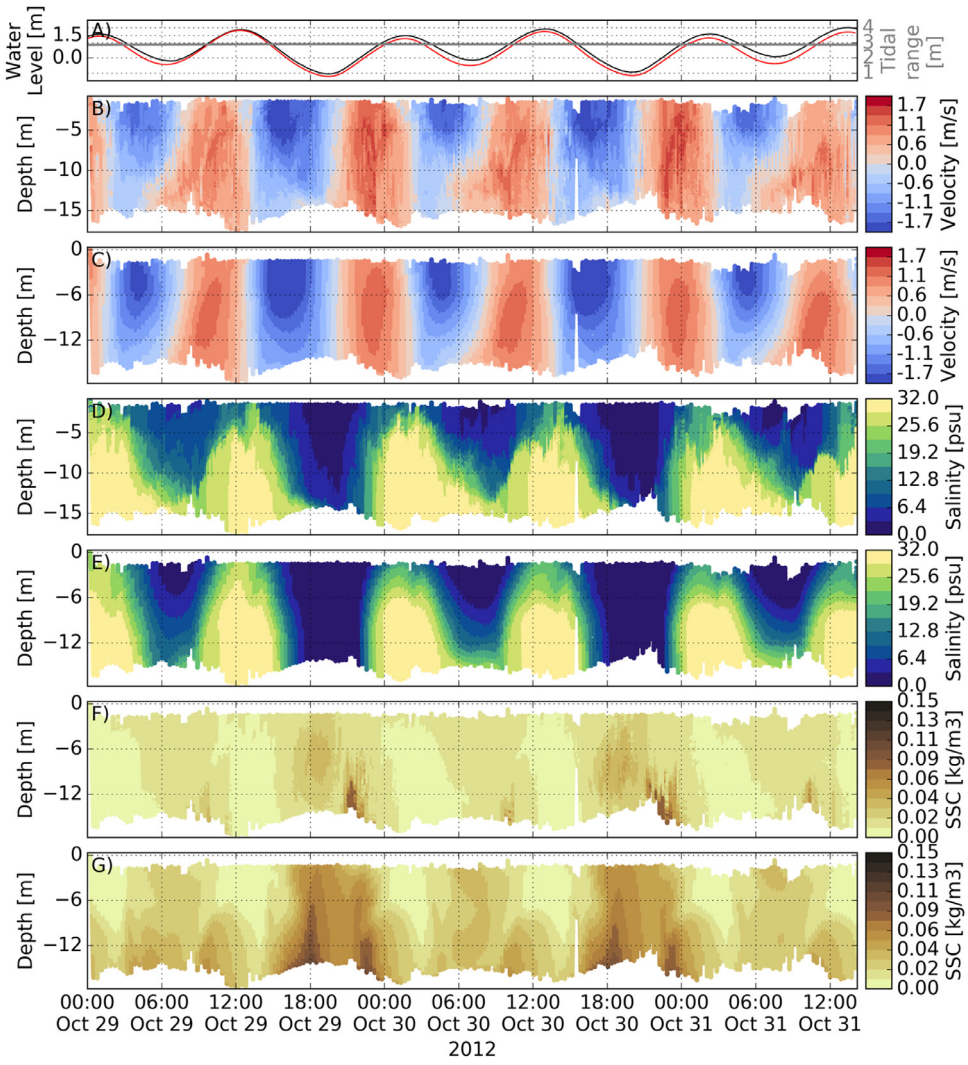


**Fig. 10.** Comparisons of observations and model results at anchorage OC2 from the Winched Profiler for water levels (A), stream-wise velocity (B), modeled stream-wise velocity (C), salinity (D), modeled salinity (E), SSC (F), and modeled SSC (G). The gray line in (A) is the tidal range.

nearly uniform velocities over the entire water column during major floods. The under-predicted salinity intrusion is reflected in the negative bias of the along channel currents (−0.15 m/s), but other skill metrics suggest good overall skill (MS = 0.87, WS = 0.97).

*4.4.2. Suspended sediment comparisons*

A few essential features characterize the observed sediment dynamics observed at OC1 (Fig. 9) and OC2 (Fig. 10). The lowest SSC are found in high-salinity waters in the salt wedge representative of sediment concentrations of the adjacent coastal area. The highest concentrations of SSC are found near the bed during floods and are associated with ETM dynamics. The concentration of SSC in the flood ETM is dependent on the semi-diurnal tidal range and the change in water elevation during the preceding ebb. During ebbs when the water column remains stratified, a patch of elevated SSC advects over the salt wedge. Concentrations in this patch are correlated with the change in water level during the ebb.

At OC1 the model captures the variability of SSC over the semi-diurnal tidal cycle and represents the salient SSC features described above. Model predicted SSC is lowest in the salt wedge and fresh waters aligning with observations (Fig. 9). The dominant SSC feature is a bottom-focused flood ETM increasing in concentration as the tidal range grows following the same pattern found in observations (Fig. 9 – See October 26 15:00, October 27 3:00, and October 28 15:00). During ebbs, the near surface SSC concentrations are greater than those below the pycnocline indicating the advection of a patch of sediment over the salt wedge as seen in observations. During large ebbs the model predicts a bottom-focused ebbing ETM trailing the salt wedge. Observations show that the water column remained more stratified than the model suggests and with the highest SSC found in a patch above the pycnocline. Despite representing all of the prominent SSC features at OC1, the model MS is negative (−0.72) suggesting that it has less predictive ability than the mean of observations, whereas other metrics suggest poor (Corr = 0.16) and moderate skill (WS = 0.41) (Table 6).

Model results at OC2 are similar to those at OC1, capturing observed trends well during floods, but less so during major ebbs (Fig. 10). As at OC1, the discrepancy between simulations and observations results from the under-prediction of salinity intrusion and retention and the over-prediction of ebbing currents. Under-prediction of salinity intrusion and retention during ebbs leads to the model predicting an ebb ETM (e.g. October 29 10:00–18:00). However, observations show that the water column remained stratified and a patch of elevated suspended sediment concentrations passed over the salt-wedge. As at OC1, the effects

**Table 7**
Performance comparison before performance enhancements for SELFE v3.1 (3.1) and after enhancements SELFE v4.0 (4.0) for a realistic hindcast simulation of the Columbia River system. *Total time* refers to wall-clock time for the entire simulation and *Time per day* refers to the wall-clock time per simulated day.

| Test | Number of simulated days | Version | Tracers | Number of processes | Total time [min.] | Time per day [min.] |
|---|---|---|---|---|---|---|
| S1 | 14 | 3.1 | T, S | 128 | 534 | 38 |
| S2 | 14 | 4.0 | T, S | 128 | 271 | 19 |
| S3 | 14 | 4.0 | T, S | 1024 | 92 | 6 |
| S4 | 2 | 3.1 | T, S, 4 tracers | 128 | 262 | 131 |
| S5 | 2 | 4.0 | T, S, 4 tracers | 128 | 67 | 32 |

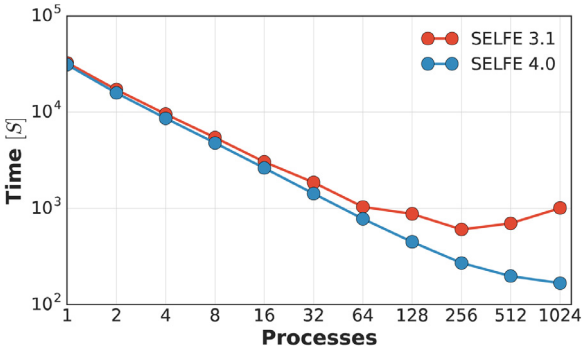


**Fig. 11.** Comparison of strong-scaling of SELFE before computational improvements (SELFE v3.1) and after (SELFE v4.0) using a realistic domain with ~89 K nodes and ~4.5 M 3D prisms on the NERSC Edison system. 1024 processes is near the limit of domain decomposition for this problem size.

of ebb tide substantially degrade the MS (−4.06) indicating poor skill, whereas other metrics indicated moderate skill (Corr = 0.69, WS = 0.57) (Table 6).

#### 4.4.3. Computational performance

We provide performance metrics of SELFE in terms of strong-scaling and time to solution for problem sizes similar to those used for this study to provide an estimate of the computational cost. The location and problem size is site specific, but provides useful insight into performance for this class of model for a realistic application.

We compare the strong-scaling performance of a previous version of the model (SELFE v3.1) documented to lack scalability (Kerr et al., 2013) and the current version (SELFE v4.0) which includes a new treatment for the linear solve for continuity and atmospheric boundary conditions. In this test we run the base hydrodynamics including temperature and salinity, but no additional tracers, on the National Energy Research Scientific Computing Center (NERSC) Edison cluster, a Cray XC30. The mesh (~89 K 2D, ~4.5 M 3D elements) and model parameters are realistic for a scientifically meaningful representation of estuarine circulation in the Columbia River estuary and are described in Section 4.2 and Table 5. The model is run for 12 simulated hours from a spun-up hotstart state derived from a hindcast simulation. The mean timings for the test on the NERSC Edison system are reported in Table 7. SELFE v3.1 scales nearly linearly up to 64 processes where it then diverges reaching the fastest time to solution using 256 processes (Fig. 11). This same limit has been found on larger grids internally and by other researchers (Kerr et al., 2013). In contrast, SELFE v4.0 scales nearly linearly to 128 processes where it begins to diverge, but continues to scale sub-linearly to 1024 processes. Use of 1024 processes is close to the upper bound of the number of processes that can be used for this problem size.

Comparing the time to solution between SELFE v3.1 and SELFE v4.0, we use the same grid model parameters as those in strong scaling test (Table 7). Two of the tests include the addition of four passive tracers which act as a proxy for sediment model simulations. Ideally we would have compared the performance using four sediment classes, but the sediment model in SELFE v3.1 was unstable and simulations would not complete. Focusing first on the results using 128 processes, we note that for purely hydro-dynamic simulations (S1 versus S3), SELFE v4.0 is twice as fast as SELFE v3.1. However, for simulations with passive tracers (S4 versus S5), SELFE v4.0 is 4 times as fast. Adding tracers slows the simulations by factor of two (S2 versus S4) for SELFE v4.0, and ~3.4 times as slow for SELFE v3.1 (S1 versus S4).

## 5. Discussion

### 5.1. Idealized tests and implications

We have shown that the SELFE sediment module represents analytical solutions, laboratory data or expected behaviors in a suite of idealized test cases, with a skill qualitatively similar to other published results, but lags the skill of the higher-order ROMS and Delft3D model in specific tests (Burchard et al., 2004; Lesser et al., 2004; Warner et al., 2008; Pinto et al., 2012).

The open channel test isolates suspended sediment dynamics in an unstratified flow by neglecting bed load transport and morphology. Model results show high sensitivity of SSC to the selection and implementation of the turbulence closure model. The native SELFE implementation of the GLS equations produce spikes in TKE near the bed and a convex profile of eddy diffusivity near the surface when the “no-slip” boundary condition is used for the momentum equation. The same characteristics are not reproduced when using the online coupled GOTM implementation of the GLS suggesting that the differences lie in the numerics and implementation for the GLS equations. As shown in previous work (Pinto et al., 2012; Warner et al., 2008) use of the GLS turbulence closure universally results in underprediction of suspended sediment against a semi-analytical solution assuming a Rouse profile. The analytical Rouse solution significantly under-predicts SSC in the upper water column compared to the semi-analytical solution highlighting uncertainty in the real behavior of sediments. The difference between these solutions is caused by model specific details of numerics and implementation, in addition to the inherent uncertainty associated with the Rouse profile. Violeau et al., (2002) found a similar spread in solutions when comparing numerical solutions using different models.

In contrast to the open channel case, the trench migration incorporates suspended sediment, bed load transport, and morphological processes in an unstratified flow. Despite the bed properties being tightly constrained by the parameters stipulated in the flume test, numerical results required extensive sensitivity tests for bottom roughness, critical stress, and erosion rate. The first difficulty encountered was optimizing the bottom roughness and time step for velocity. Attempts at using the same time step and grid resolution as specified in Warner et al., (2008) and

Pinto et al., (2012) resulted in poor representation of velocity. Sensitivity analysis of time step resulted in an optimal time step of 0.375 s compared to 0.05 s used in Pinto et al., (2012). Despite this optimization, qualitative comparisons of velocity profiles between SELFE and ROMS (Warner et al., 2008) and Delft3D (Lesser et al., 2004) suggest that the lower-order SELFE is not as skilled at representing horizontal velocity, particularly within the trench. The effects of the deviation between observed and modeled velocity on SSC are evident in Fig. 3 at stations 2–4. Comparisons between predicted trench migration and observations suggest that SELFE is representing bed load transport and morphodynamics reasonably well. The location of the trench entrance and maximum depth is similar to observations, but the exit of the trench shows a gradual incline not seen in observations as shown in other tests (Lesser et al., 2004; Warner et al., 2008; Pinto et al., 2012). Unlike the open channel case, the SSC and migration of the channel is much less dependent on the selection of the turbulence closure model because interactions between the bed and suspended sediment dominate the variability induced by differing representations of vertical mixing. The implication is that sediment modeling in realistic environments is likely to be dominated by bed dynamics and not selection of turbulence closure. Model skill for the bed, as measure by quantitative error metrics, is poor despite good qualitative agreement. This suggests that: traditional metrics of skill are inadequate to assess the ability of a model to capture sediment related processes and sediment model skill lags that of hydrodynamics.

The idealized tidal estuary with stratification is a critical test of the predictive skill of estuarine sediment models. A number of studies have shown that density effects substantially alter sediment transport and assessing the ability of a model to represent these interactions is critical in stratified regions (Burchard & Flöser, 2008; Elias et al., 2012). Sensitivity analysis to the imposition of boundary conditions for density suggest a broad solution space, most of which do not result in a stable, periodic solution as has been described in previous studies (Warner et al., 2008). While the model is able to reproduce estuarine circulation and sediment dynamics that adhere to conceptual understanding and theory (Dyer, 1998), there is no means of quantifying the results although comparison with other published results suggest qualitative agreement (Burchard et al., 2004; Warner et al., 2008). The lack of laboratory observations for a similar test case represents a critical research gap.

### 5.2. Model skill in realistic scenario and limitations

Application of the model to a realistic hindcast scenario reveals that the sediment model is capable of representing sediment dynamics detailed by field instrumentation when optimized for skill against time series observations from the SATURN observatory (Fig. 9). From the perspective of observations at these stations and fixed depths, the sediment model is able to capture the variability and concentrations of suspended sediments. Comparisons between model results and field observations over the entire water column reveal limitations of both the hydrodynamics and suspended sediments obfuscated in point-wise time series comparisons (Figs. 9 and 10). At the North Channel cruise station OC1, three dominant features in suspended sediment are represented, but concentrations in the upper water column are slightly overestimated (Fig. 9). Elevated SSC in the upper water column corresponding with the growing tidal range indicates that model is accurately representing the increase of SSC in the system resulting from enhanced erosion. Model SSC is overestimated during ebbs near the bed corresponding with underprediction of stratification and overprediction of currents and shear. The underprediction of stratification during ebbs corresponds with the phase difference of the tide in simulations. Analysis of two-dimensional barotropic and three-dimensional baroclinic simulations indicate that baroclinicity substantially affects elevation and that elevation errors are related to the underprediction of the baroclinic pressure gradient (not shown). The implications of underpredicting baroclinicity on suspended sediment dynamics are more apparent at OC2 (Fig. 10). During larger ebb tides, the model over-predicts the advection and mixing of the salt wedge resulting in a fresh water column at OC2 distorting the vertical location of suspended sediments. The dichotomy between model skill reflected in fixed station time series and the profiles of the water column exposes the difficulty and limitation of assessing model skill. Comparisons at fixed stations suggest the model captures variability of sediment. Similarly, the tidal variability of SSC are represented with comparisons from shipborne profiles, but show that the model completely misses the vertical distribution of suspended sediment sediments when stratification is not accurately represented during ebb tides. This highlights both the limits of the model and the limits of using fixed depth time series to assess sediment model skill and to describe suspended sediment in a stratified, dynamic estuary.

Sediment skill in our application is similar to studies using other models in other systems. As a stringent recent example, the range of Murphy Score ($-4.06$ to $-0.72$) for SSC at the OC1, OC2, and SATURN stations is similar to those reported by Ralston et al., (2013) ($-5.8$ to 0.39) in the Skagit Bay located within the Puget Sound, USA. In that study 3 out of 5 stations had negative MS. Comparing correlation coefficients for SSC, the values obtained here are only modestly better (0.16–0.69) than those found by Ralston et al., (2013) (0.12–0.4). de Nijs & Pietrzak (2012) reported similar Willmott Scores (0.12–0.48). Skill for simulations of sediments continues to lag that of simulations of elevation, velocity, or salinity, highlighting the limitations and uncertainty of sediment modeling. Although much lower than skill measurements of elevation, velocity, or salinity, the model skill here is similar to results in other systems with other models, highlighting the limitations and uncertainty of contemporary sediment models especially when evaluated with rigorous skill metrics such as the Murphy Score.

The skill metrics used here are useful in assessing the predictive ability, but fail to comprehensively describe how well the model is representing sediment processes. The Murphy Scores at the fixed stations indicate that the model is no better than taking the mean of observations (the reference used for that metric), but the correlation coefficient and Willmott score suggest that the model is at least moderately skilled (Table 6). Skill metrics for OC1 and OC2 are similar, but the correlation coefficient and the Willmott score counter-intuitively suggest that the model is more skilled at OC2 than OC1. The critical aspect of the uncertainty in the conversion from NTU to SSC is not captured in these metrics. Nor do these metrics measure any form of feature similarity such as wavelets (Saux et al., 2012) or self-organizing maps (Vilibić et al., 2016). Development of a more comprehensive feature-focused assessment of sediment model skill including uncertainty would ameliorate some of the short-comings of the current skill score assessment methodology.

Specific skill measures aside, missing from the sediment model are a number of processes that may explain lack of sediment skill. The aggregation of fine sediment through flocculation contributes to the variability of the density, size distribution, and settling velocity of material associated with ETM in the Columbia River estuary (Reed & Donovan, 1994). The precise mechanisms leading to flocculation remain uncertain and even the descriptive properties associated with it including constituent material composition and time scales of aggregation and disaggregation remain open questions. A number of mechanisms to incorporate the effects of flocculation on settling velocity have been proposed dependent on local salinity (Lesser et al., 2004) and various representations

of SSC and shear (Van Leussen, 1988; Whitehouse et al., 2000; Winterwerp et al., 2006; Baugh & Manning, 2007; Soulsby et al., 2013). Uncertainty in both expected behavior and characteristics of flocs for the Columbia River system discouraged application of these methods in this paper.

Shortwaves have been documented to cause and enhance erosion through a number of processes (Maa & Mehta, 1990; Le et al., 2000) and are known to alter mixing fields (Kularatne & Pattiaratchi, 2008). The mouth and region outside of the Columbia estuary are high energy wave environments, but currents and sediment transport are dominated by mean advection with minor contributions from winds and waves (Elias et al., 2012). Given the minor contribution of waves to sediment transport near the mouth and the focus of this work further upstream in the stratified estuary where wave effects are less intense, we have chosen to neglect wave effects. This choice should be revisited once more important hydrodynamic model limitations, such as regime-dependent underprediction of salinity intrusion (Kärnä et al., 2015), have been addressed.

## 6. Conclusions

Using idealized tests, we have validated an unstructured grid sediment model capable of reproducing suspended sediment dynamics, bed load transport, and associated morphodynamics forming a benchmark for three-dimensional sediment models. Despite being relatively well constrained, substantial sensitivity studies were required to find the optimal solution to these tests highlighting the uncertainty associated with sediment modeling. In our experience, critical details to reproduce these tests are frequently missing and we have taken efforts to provide what we believe to be sufficient details to reproduce including making the tests publically available (Lopez & Baptista, 2016).

We have shown that the sediment model is capable of representing sediment dynamics in the energetic Columbia River estuary. Although the model was tuned to optimize model skill against observations, the model missed the vertical placement of suspended sediment when the hydrodynamics underestimated stratification. The persistent underprediction of stratification in the Columbia River, in spite of substantial prior work, is a recognition that circulation modeling itself has limitations. However, sediment skill lags that of hydrodynamics because inaccuracies in predicted hydrodynamics are compounded with uncertainty from missing processes, process simplification, and parameterization. Despite these limitations, the sediment model reproduces sediment dynamics in the Columbia River estuary. In particular, the model is able to reproduce elevated concentrations of suspended sediments near the bed during flood and ebb tides collocated with the upstream limit of salinity intrusion and captures the patch of elevated SSC over the salt wedge when stratification is sufficiently represented by the hydrodynamics. In this sense, the model is a useful tool for studying ETM dynamics in the Columbia River estuary. Finally, we note that previously described scalability problems with SELFE have been partially ameliorated with the current version with the model able to scale beyond 256 cores.

## Acknowledgments

We extend gratitude to the Astoria Field Team (Oregon Health & Science University) for the maintenance of all SATURN stations. We would like to thank the captain and crew of the *R/V* Oceanus, CMOP scientists, and chief scientist Byron Crump (Oregon State University) for the collection of data. Our modeling benefited from comments and recommendations from multi-institutional CMOP modeling team, especially those of Drs. Yvette Spitz (Oregon State University) and Tuomas Kärnä (Oregon Health & Science University). This work was supported by the DOE CSGF, grant number DOE CSGF DE-FG02-97ER25308. The National Science Foundation partially supported this research through cooperative agreement OCE-0424602. The National Oceanic and Atmospheric Administration (NA11NOS0120036), Bonneville Power Administration (00062251) and Corps of Engineers (AB-133F-12-SE-2046; W9127N-12-2-007; and G13PX01212) provided partial motivation and additional support.

This work used the National Energy Research Scientific Computing Center (NERSC) a DOE Office of Science User Facility supported by the Office of Science of the U.S. Department of Energy under Contract No. DE-AC02-05CH11231, as well as the Extreme Science and Engineering Discovery Environment (XSEDE), National Science Foundation grant number ACI-1053575.

## Appendix

The semi-analytical solutions to the open channel case in Section 4.1 are derived below and are based on (Warner et al., 2008) and extended to analytical solutions (J.Paul Rinehimer, personal communication). The key to deriving analytical and semi-analytical solutions to the open channel test case is to assume that the eddy viscosity profile has a parabolic shape:

$$K_M = k u_* z\left(1 - \frac{z}{D}\right) \tag{13}$$

where $u_*$ is the friction velocity, $z$ is the height above the bed, and $H$ is the height of the water column. By assuming a Prandlt number of 0.8 that is reasonable for the flow conditions, the eddy diffusivity is imposed as a constant where $K_H = K_M \,/\, 0.8 = 0.49$. The analytical velocity profile is derived from the logarithmic velocity profile

$$u(z) = \frac{1}{\kappa}\left(\frac{z}{z_0}\right)u_* \tag{14}$$

where $\bar{u}$ is the depth average velocity in m s$^{-1}$, $u(z)$ is the velocity at $z$ m above the bed, $\kappa = 0.41$ is the von Karman constant, $z_0 = 0.0053$ is the bottom roughness, and $u_* = 0.0625$ is the friction velocity.

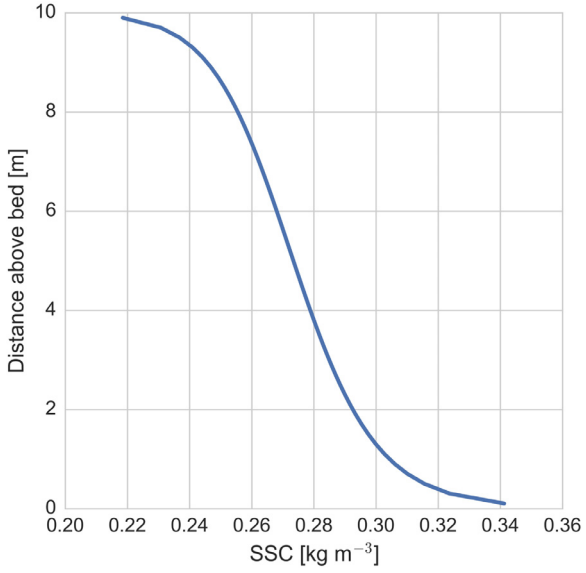


**Fig. 12.** Profile of Rouse solution to open channel case using $z_0 = 0.0053$ assuming a no-slip bottom boundary condition, a logarithmic velocity profile, a Prandlt number of 0.8.

Because the channel is assumed to be in a steady state, the suspended sediment concentrations can be predicted assuming a Rouse profile with the Rouse parameter, $P$, given by

$$P = \frac{w_s}{\alpha \kappa u_*} \tag{15}$$

where $w_s$ is the sediment settling velocity, $\alpha$ is the Prandlt number, $\kappa$ is the von Karman constant, and $u_*$ is the friction velocity. Applying the eddy diffusivity, $K_H$, the prescribed erosion rate, $E$, and settling velocity for the suspended sediment, $w_s$ we can solve for the suspended sediment concentration

$$C(z) = \frac{E}{w_s}\left[\frac{z}{z_0}\frac{(H-z_0)}{(H-z)}\right]^{-P} \tag{16}$$

at height $z$ above the bed with reference $z_0 = 0.0053$ for the test case. The results are shown in Fig. 12.

## References


Baptista, A.M., Seaton, C., Wilkin, M., Riseman, S., Turner, P., Karna, T., Megler, V., 2015. Infrastructure for collaborative estuarine science and societal applications in the Columbia River, United States. Front. Earth Sci. 9 (4), 659–682. doi:10.1007/s11707-015-0540-5.

Barron, C.N., Kara, A.B., Martin, P.J., Rhodes, R.C., Smedstad, L.F., 2006. Formulation, implementation and examination of vertical coordinate choices in the Global Navy Coastal Ocean Model (NCOM). Ocean Modell. 11 (3–4), 347–375. doi:10.1016/j.ocemod.2005.01.004.

Baugh, J.V, Manning, A.J., 2007. An assessment of a new settling velocity parameterisation for cohesive sediment transport modeling. Cont. Shelf Res. 27 (13), 1835–1855. doi:10.1016/j.csr.2007.03.003.

Brenon, I., Le Hir, P., 1999. Modelling the turbidity maximum in the Seine estuary (France): identification of formation. Estuar. Coast. Shelf Sci. 49 (4), 525–544. doi:10.1006/ecss.1999.0514.

Burchard, H., Baumert, H., 1998. The formation of estuarine turbidity maxima due to density effects in the salt wedge. A hydrodynamic process study. J. Phys. Oceanogr. 28 (2), 309–321. doi:10.1175/1520-0485(1998)028⟨0309:TFOETM⟩2.0.CO;2.

Burchard, H., Bolding, K., Villarreal, M.R., 2004. Three-dimensional modelling of estuarine turbidity maxima in a tidal estuary. Ocean Dyn. 54 (2), 250–265. doi:10.1007/s10236-003-0073-4.

Burchard, H., Floser, G., Staneva, J.V, Badewien, T.H., Riethmuller, R., 2008. Impact of density gradients on net sediment transport into the Wadden Sea. J. Phys. Oceanogr. 38 (3), 566–587. doi:10.1175/2007jpo3796.1.

Casulli, V., Cheng, R.T., 1992. Semi-implicit finite difference methods for three-dimensional shallow water flow. Int. J. Numer. Methods Fluids 15 (6), 629–648. doi:10.1002/fld.1650150602.

Chawla, A., Jay, D.A., Baptista, A.M., Wilkin, M., Seaton, C., 2008. Seasonal variability and estuary – shelf interactions in circulation dynamics of a river-dominated estuary. Estuar. Coast. 31 (2), 269–288. doi:10.1007/s12237-007-9022-7.

Chen, C., Liu, H., Beardsley, R.C., 2003. An unstructured grid, finite-volume, three-dimensional, primitive equations ocean model: application to coastal ocean and estuaries. J. Atmos. Oceanic Technol. 20 (1), 159–186. doi:10.1175/1520-0426(2003)020⟨0159:AUGFVT⟩2.0.CO;2.

de Nijs, M.J., Pietrzak, J.D., 2012. Saltwater intrusion and ETM dynamics in a tidally-energetic stratified estuary. Ocean Modell. 49, 60–85. doi:10.1016/j.ocemod.2012.03.004.

Dyer, K.R., 1998. Estuaries: A Physical Introduction. Estuarine and Coastal Marine Science, 2nd ed. John Wiley & Sons, Chichester.

Elias, E.P.L., Gelfenbaum, G., Van der Westhuysen, A.J., 2012. Validation of a coupled wave-flow model in a high-energy setting: the mouth of the Columbia River. J. Geophys. Res. Oceans 117 (C9). doi:10.1029/2012JC008105.

Fain, A.M.V., Jay, D.A., Wilson, D.J., Orton, P.M., Baptista, A.M., 2001. Seasonal and tidal monthly patterns of particulate matter dynamics in the Columbia River estuary. Estuaries 24 (5), 770. doi:10.2307/1352884.

Ferguson, C.M., Coote, B.G., Ashbolt, N.J., Stevenson, I.M., 1996. Relationships between indicators, pathogens and water quality in an estuarine system. Water Res. 30 (9), 2045–2054. doi:10.1016/0043-1354(96)00079-6.

Fortunato, A.B., Oliveira, A., 2004. A modeling system for tidally driven long-term morphodynamics. J. Hydraul. Res. 42 (4), 426–434. doi:10.1080/00221686.2004.9641210.

Fox, D., Bell, S., Nehlsen, W., Damron, J., 1984. Atlas of Physical and Biological Characteristics of the Columbia River Estuary. Columbia River Estuary Data Development Program, Astoria, OR.

Fringer, O.B., Gerritsen, M., Street, R.L., 2006. An unstructured-grid, finite-volume, nonhydrostatic, parallel coastal ocean simulator. Ocean Modell. 14 (3–4), 139–173. doi:10.1016/j.ocemod.2006.03.006.

Harris, C.K., Wiberg, P.L., 2001. A two-dimensional, time-dependent model of suspended sediment transport and bed reworking for continental shelves. Comput. Geosci. 27 (6), 675–690. doi:10.1016/S0098-3004(00)00122-9.

Kärnä, T., Baptista, A.M., Lopez, J.E., Turner, P.J., Mcneil, C., Sanford, T.B., 2015. Numerical modeling of circulation in high-energy estuaries: a Columbia River estuary benchmark. Ocean Modell. 88, 54–71. doi:10.1016/j.ocemod.2015.01.001.

Kerr, P.C., Donahue, A.S., Westerink, J.J., Luettich, R.A., Zheng, L.Y., Weisberg, R.H., Cox, A.T., 2013. U.S. IOOS coastal and ocean modeling testbed: inter-model evaluation of tides, waves, and hurricane surge in the Gulf of Mexico. J. Geophys. Res. Oceans 118 (10), 5129–5172. doi:10.1002/jgrc.20376.

Kularatne, S., Pattiaratchi, C., 2008. Turbulent kinetic energy and sediment resuspension due to wave groups. Cont. Shelf Res. 28 (6), 726–736. doi:10.1016/j.csr.2007.12.007.

Le Hir, P., Roberts, W., Cazaillet, O., Christie, M., Bassoullet, P., Bacher, C., 2000. Characterization of intertidal flat hydrodynamics. Cont. Shelf Res. 20 (12–13), 1433–1459. doi:10.1016/S0278-4343(00)00031-5.

Lesser, G.R., Roelvink, J.A., Van Kester, J.A.T.M., Stelling, G.S., 2004. Development and validation of a three-dimensional morphological model. Coastal engineering 51 (8), 883–915. doi:10.1016/j.coastaleng.2004.07.014.

Lin, J., Kuo, A.Y., 2003. A model study of turbidity maxima in the York River estuary, Virginia. Estuaries 26 (5), 1269–1280. doi:10.1007/BF02803629.

Lopez, J.E., & Baptista, A.M. (2016). SELFE sediment model benchmark in the Columbia River estuary. [Data set]. Zenodo. doi:10.5281/zenodo.60071.

Maa, J.P.-Y., Mehta, A.J., 1990. Soft mud response to water waves. J. Waterw. Port, Coast. Ocean Eng. 116 (5), 634–650. doi:10.1061/(ASCE)0733-950X(1990)116:5(634).

Meade, R.H., 1972. Transport and deposition of sediments in estuaries. Geol. Soc. Am. Mem. 133, 91–120. doi:10.1130/MEM133-p91.

Meyer-Peter, E., Müller, R., 1948. Formulas for bed-load transport. In: Proceedings of the 2nd Meeting of the International Association of Hydraulic Research, pp. 39–64. http://doi.org/1948-06-07.

Myers, E.P., Baptista, A.M., 2001. Inversion for tides in the Eastern North Pacific Ocean. Adv. Water Res. 24 (5), 505–519. doi:10.1016/S0309-1708(00)00041-5.

Pinto, L., Fortunato, A.B., Zhang, Y., Oliveira, A., Sancho, F.E.P., 2012. Development and validation of a three-dimensional morphodynamic modelling system for non-cohesive sediments. Ocean Modell. doi:10.1016/j.ocemod.2012.08.005.

Ralston, D.K., Geyer, W.R., Lerczak, J.A., Scully, M., 2010. Turbulent mixing in a strongly forced salt wedge estuary. J. Geophys. Res. Oceans 115 (12), 1–21. doi:10.1029/2009JC006061.

Ralston, D.K., Geyer, W.R., Traykovski, P.A., Nidzieko, N.J., 2013. Effects of estuarine and fluvial processes on sediment transport over deltaic tidal flats. Cont. Shelf Res. 60, S40–S57. doi:10.1016/j.csr.2012.02.004.

Ralston, D.K., Geyer, W.R., Warner, J.C., 2012. Bathymetric controls on sediment transport in the Hudson River estuary: lateral asymmetry and frontal trapping. J. Geophys. Res. 117 (C10), C10013. doi:10.1029/2012JC008124.

Reed, D.J., Donovan, J., 1994. The character and composition of the Columbia River estuarine turbidity maximum. Chang. Fluxes Estuar. Implic. Sci. Manag. 445–450. doi:10.1161/01.HYP.7.3_Pt_2.I49.

Rogers, E., DiMego, G., Black, T., Ek, M., Ferrier, B., Gayno, G., Wu, W., 2009. The NCEP North American mesoscale modeling system: recent changes and future plans. In: Proceedings of the 23rd Conference on Weather Analysis and Forecasting/19th Conference on Numerical Weather Prediction. Omaha, Nebraska.

Sanford, T.B., McNeil, C., Shcherbina, A.Y., Litchendorf, T.M., Karna, T., Lopez, J.E., & Baptista, A.M. (2015). CMOP 2012 AUV-WP Columbia River estuary benchmark data set [Data set]. Zenodo. http://doi.org/10.5281/zenodo.13782.

Saux Picart, S., Butenschén, M., Shutler, J.D., 2012. Wavelet-based spatial comparison technique for analysing and evaluating two-dimensional geophysical model fields. Geosci. Model Dev. 5 (1), 223–230. doi:10.5194/gmd-5-223-2012.

Sherwood, C.R., Creager, J.S., 1990. Sedimentary geology of the Columbia River estuary. Prog. Oceanogr. doi:10.1016/0079-6611(90)90003-K.

Soulsby, R.L., Manning, A.J., Spearman, J., Whitehouse, R.J.S., 2013. Settling velocity and mass settling flux of flocculated estuarine sediments. Mar. Geol. 339, 1–12. doi:10.1016/j.margeo.2013.04.006.

Sutherland, J., Peet, A.H., Soulsby, R.L., 2004. Evaluating the performance of morphological models. Coastal Eng. 51 (8–9), 917–939. doi:10.1016/j.coastaleng.2004.07.015.

Umlauf, L., Burchard, H., 2005. Second-order turbulence closure models for geophysical boundary layers. A review of recent work. Cont. Shelf Res. 25 (7–8 Special Issue), 795–827. doi:10.1016/j.csr.2004.08.004.

Van Leussen, W., 1988. Aggregation of particles, settling velocity of mud flocs a review. In: Physical Processes in Estuaries. Springer, Berlin, pp. 347–403. doi:10.1007/978-3-642-73691-9_19.

van Rijn, L.C., 1986. Mathematical modeling of suspended sediment in nonuniform flows. J. Hydraul. Eng. 112 (6), 433–455. doi:10.1061/(ASCE)0733-9429(1986)112:6(433).

van Rijn, L.C., 1993. Principles of Sediment Transport In Rivers, Estuaries And Coastal Seas, (Vol. 1006). Amsterdam, Aqua publications, pp. 1–17.

van Rijn, L.C., Walstra, D.-J.R., van Ormondt, M., 2007. Unified view of sediment transport by currents and waves. IV: application of morphodynamic model. J. Hydraul. Eng. 133 (7), 776–793. doi:10.1061/(ASCE)0733-9429(2007)133:7(776).

Vilibić, I., Šepić, J., Mihanović, H., Kalinić, H., Cosoli, S., Janeković, I., Ivanković, D., 2016. Self-organizing maps-based ocean currents forecasting system. Sci. Rep. 6, 22924. doi:10.1038/srep22924.

Violeau, D., Bourban, S., Cheviet, C., Markofsky, M., Petersen, O., Roberts, W., Weilbeer, H., 2002. Numerical simulation of cohesive sediment transport : intercomparison of several numerical models. Fine Sedim. Dyn. Mar. Environ. 75–89. doi:10.1016/S1568-2692(02)80009-2.

Warner, J.C., Sherwood, C.R., Geyer, W.R., 2007. Sensitivity of estuarine turbidity maximum to settling velocity, tidal mixing, and sediment supply. Proc. Mar. Sci. 8, 355–376. doi:10.1016/S1568-2692(07)80022-2.

Warner, J.C., Sherwood, C.R., Signell, R.P., Harris, K., Arango, H.G., Harris, C.K., Arango, H.G., 2008. Development of a three-dimensional, regional, coupled wave, current, and sediment-transport model. Comput. Geosci. 34 (10), 1284–1306. doi:10.1016/j.cageo.2008.02.012.

Warrick, J.A., 2015. Trend analyses with river sediment rating curves. Hydrol. Process. 29 (6), 936–949. doi:10.1002/hyp.10198.

Whitehouse, R., Richard, S., Roberts, W., Mitchener, H., 2000. Dynamics of Estuarine Muds. Thomas Telford Ltd. doi:10.1680/doem.28647.

Willmott, C.J., 1981. On the validation of models. Phys. Geogr. 2 (2), 184–194. doi:10.1080/02723646.1981.10642213.

Winterwerp, J.C., Manning, A.J., Martens, C., de Mulder, T., Vanlede, J., 2006. A heuristic formula for turbulence-induced flocculation of cohesive sediment. Estuar. Coast. Shelf Sci. 68 (1–2), 195–207. doi:10.1016/j.ecss.2006.02.003.

Zhang, Y., Baptista, A.M., 2008. SELFE: a semi-implicit Eulerian–Lagrangian finite-element model for cross-scale ocean circulation. Ocean Modell. 21 (3), 71–96. doi:10.1016/j.ocemod.2007.11.005.

Zhang, Y.J., Ye, F., Stanev, E.V, Grashorn, S., 2016. Seamless cross-scale modeling with SCHISM. Ocean Modell. 102, 64–81. doi:10.1016/j.ocemod.2016.05.002.